ChemPubSoc Europe
DOI: 10.1002/cptc.201700162
CHEMPHOTOCHEM Articles

Special Issue

Understanding Two Different Structures in the Dark Stable State of the Oxygen-Evolving Complex of Photosystem II: Applicability of the Jahn–Teller Deformation Formula

Mitsuo Shoji,[a] Hiroshi Isobe,[b] Ayako Tanaka,[c] Yoshimasa Fukushima,[c] Keisuke Kawakami,[c] Yasufumi Umena,[c] Nobuo Kamiya,[c] Takahito Nakajima,[d] and Kizashi Yamaguchi*[d, e, f]

Tanaka et al. (*J. Am. Chem. Soc.*, **2017**, *139*, 1718) recently reported the three-dimensional (3D) structure of the oxygen evolving complex (OEC) of photosystem II (PSII) by X-ray diffraction (XRD) using extremely low X-ray doses of 0.03 and 0.12 MGy. They observed two different 3D structures of the $CaMn_4O_5$ cluster with different hydrogen-bonding interactions in the S_1 state of OEC keeping the surrounding polypeptide frameworks of PSII the same. Our Jahn–Teller (JT) deformation formula based on large-scale quantum mechanics/molecular mechanics (QM/MM) was applied for these low-dose XRD structures, elucidating important roles of JT effects of the Mn^{III} ion for subtle geometric distortions of the $CaMn_4O_5$ cluster in OEC of PSII. The JT deformation formula revealed the similarity between the low-dose XRD and damage-free serial femtosecond X-ray diffraction (SFX) structures of the $CaMn_4O_5$ cluster in the dark stable state. The extremely low-dose XRD structures were not damaged by X-ray irradiation. Implications of the present results are discussed in relation to recent SFX results and a blue print for the design of artificial photocatalysts for water oxidation.

1. Introduction

A number of experimental studies for oxygen evolving complex (OEC) of photosystem II (PSII) have been performed using several kinds of experimental techniques.[1,2] Structural parameters, particularly Mn-Mn distances, of the $CaMn_4O_5$ cluster in OEC of PSII have been investigated by the extended X-ray absorption fine structure (EXAFS).[3–10] On the other hand, X-ray diffraction (XRD) experiments[11–19] play an important role for elucidation of complex, three-dimensional (3D) structures of transition metal-containing enzymes such as OEC of PSII, providing structural bases for successive investigations by spectroscopic methods such as EPR and FTIR.[1,2] However a critical issue of the XRD[11–19] for redox-active OEC of PSII is the radiation damage with intense synchrotron radiation as compared with EXAFS.[3–10] In the past six years, serial femtosecond X-ray (SFX) diffraction method, known as "diffraction-before-degradation", using the X-ray free-electron laser (XFEL)[20–29] have been developed to obtain damage-free XRD structures of redox-active enzymes such as OEC of PSII. On the other hand, low dose XRD experiments have been also desired for suppression of the X-ray damage.[6,7] Tanaka et al.[30] recently reported the 3D structures of the $CaMn_4O_5$ cluster in OEC of PSII by XRD using extremely low X-ray doses of 0.03 and 0.12 MGy, for which the external Mn reductions were estimated to be less than 1 and 3.5 (%), respectively.[6,7,30] They observed that geometrical structures of the A-monomer were different from those of the B-monomer in the dimer units of both 5B5E with 0.03 MGy and 5B66 with 0.12 MGy XRD results even in the S_1 state of the Kok cycle,[31,32] although the surrounding polypeptide frameworks of PSII were the same.[30]

In the past decade we have performed broken-symmetry (BS) hybrid DFT (UB3LYP) calculations[33–36] of the $CaMn_4O_5$ cluster in OEC of PSII starting from the 3D XRD (0.43 MG) structure[18] for theoretical investigation of geometrical, electronic and spin structures of OEC of PSII. The UB3LYP calculations

[a] *M. Shoji*
Center of Computational Sciences
Tsukuba University
Tsukuba, Ibaraki 305–8577 (Japan)
[b] *H. Isobe*
Graduate School of Natural Science and Technology
Okayama University
Okayama, 700–8530 (Japan)
[c] *A. Tanaka, Y. Fukushima, K. Kawakami, Y. Umena, Prof. N. Kamiya*
The OUC Advanced Research Institute for Natural Science and Technology (OCARNA), Osaka City University
Osaka, 558–8585 (Japan)
[d] *T. Nakajima, Prof. K. Yamaguchi*
Riken Advanced Institute for Computational Science
Chuo-Ku, Kobe, Hyogo, 650-0047 (Japan)
[e] *Prof. K. Yamaguchi*
Institute for Nanoscience Design, Osaka University
Toyonaka, Osaka, 560–8531 (Japan)
E-mail: yama@chem.sci.osaka-u.ac.jp
[f] *Prof. K. Yamaguchi*
Handairigaku Techno-Research
Toyonaka, Osaka 560-0043 (Japan)

Supporting Information for this article can be found under: https://doi.org/10.1002/cptc.201700162.

Special Issue An invited contribution to a Special Issue on Artificial Photosynthesis.

were performed for total 48 (=8×6) valence configurations obtained by 8 spin states for 6 mixed valence structures (see SV).[37] The energy diagrams for all the configurations elucidated that the ground valence configuration of the cluster in the dark stable S_1 state was the $Ca^{II}Mn^{III}_{4(a)}Mn^{IV}_{3(b)}Mn^{IV}_{2(c)}Mn^{III}_{1(d)}$, that was abbreviated as (3443). Moreover the DFT calculations elucidated that the nature of the Mn_4–$O_{(5)}$–Mn_1 bond of the cluster was labile,[33] indicating structural symmetry breaking (SSB)[35,36] because of the Jahn–Teller (JT) effects of the $Mn^{III}_{4(a)}$ ion. Full geometry optimizations of OEC of PSII by large-scale QM/MM methods[37,38] indeed elucidated four different topological structures based on the JT effects as illustrated in the Supporting Information Figure S1 (see SII.1). An estimation formula[39] of the JT deformations of the cluster also emerged on the basis of a number of the optimized geometries by QM and QM/MM,[33–39] together with available experimental geometrical parameters of manganese oxides clusters. In this paper, we apply our JT deformation formula for two different S_1 structures by the low-dose XRD experiments of Tanaka et al.,[30] proposing a unified view of the EXAFS,[3–10] XRD[11–19] and XFEL[27–29] structures and theoretical models[33–44] of the S_1 state of OEC of PSII. Implication of present results is discussed in relation to recent SFX results and a blue print for the design of artificial photo-catalysts using abundant 3d-transition metals.

2. Theoretical Background

2.1. Structural Symmetry Breaking of the $CaMn_4O_5$ Cluster in the OEC of PSII

The high-resolution XRD[18] experiments first elucidated the 3D structure of the $CaMn_4O_5$ cluster with almost central (C) conformation, as illustrated in Figure S1. Our QM and QM/MM computations[33–39] revealed slightly right (C_R)- and left (C_L)-elongated quasi-central structures as well as right (R)- and left (L)-opened structures of the $CaMn_4O_5$ cluster of OEC (see Figure S1). The structural symmetry breaking (SSB) parameter defined by using the distances of the $Mn_{1(d)}$–$O_{(5)}$ and $Mn_{4(a)}$–$O_{(5)}$ bonds is as follows [Eq. (1)]:[37–39]

$$\delta = [R(Mn_{1(d)}-O_{(5)})-R(Mn_{4(a)}-O_{(5)})/2 \quad (1)$$

The δ-value was 0.05 Å for the 3ARC XRD central (C) structure[18] of the $CaMn_4O_5$ cluster. The δ-values were 0.12 and 0.16 (Å) for A- and B-monomers of 3WU2,[18] namely refined 3ARC structure, indicating the C_R structure. The δ-values for 4UB6A, 4UB6B, 4UB8A and 4UB8B by the damage-free XFEL method[27] were 0.20, 0.23, 0.15 and 0.20 (Å) respectively, exhibiting the C_R structure in Figure S1. Thus the SSB parameters for 3WU2, 4UB6 and 4UB8 are smaller than 0.25 Å.

The SSB (δ) parameter was 0.71 Å for the full-optimized low-spin (LS) S_1 structure of the $CaMn_4O_5$ cluster by large-scale QM/MM method[37,38] on the assumption that the $O_{(5)}$ site was oxygen dianion (O^{2-}), indicating the R-structure in Figure S1. The optimized S_1-structures obtained by other and our groups under the same assumption of $O_{(5)}$=O^{2-} were also the R-structure.[40–47] The large δ-value (>0.5 Å) obtained by the theoretical calculations is one of the reasons for the claim[44,46] that the XFEL structure with small δ-value (<0.25 Å)[27] might be the S_0 structure induced by the radical addition to the $CaMn_4O_5$ cluster. On the other hand, we have shown that the C_R structure for the S_1 state can be reproduced under the assumption of the protonation of the $O_{(5)}$ site, namely $O_{(5)}$=OH^-[35–39] and/or the rotation of the JT deformation axis ($d_{z^2}\rightarrow d_{x^2}$) for $O_{(5)}$=O^{2-}.[39] Therefore, theoretical analysis of the damage-free low dose XRD structure[30] is very important for elucidation of the most plausible S_1 structure and scope and reliability of the XFEL[27] and SFX structures.[28,29]

2.2. Theoretical Modeling of Structural Symmetry Breaking in the $CaMn_4O_5$ Cluster

Our QM and QM/MM calculations[33–39] of OEC in PSII revealed that the $Mn_{4(a)}$–$Mn_{3(b)}$ distance was correlated with $Mn_{4(a)}$–$O_{(5)}$ distance in the $CaMn_4O_5$ cluster of OEC of PSII. We have already presented a practical estimation equation[37–39] of the $Mn_{4(a)}$–$Mn_{3(b)}$ distance by the use of the $Mn_{4(a)}$–$O_{(5)}$ distance (see Figure S2 in SII.1) as follows [Eq. (2)]:

$$R(Mn_{4(a)}-Mn_{3(b)}) = 2.80 + x/2n \quad (2)$$

where the deformation parameter x is defined by [Eqs. (3a) and (3b)]:

$$R(Mn_{4(a)}-O_{(5)}) = 2.18 + x \quad (3a)$$

$$R(Mn_{1(d)}-O_{(5)}) = 2.88-x\ (\text{Å unit}). \quad (3b)$$

The n-values were taken to be 1 for $O_{(5)}$=$OH^{-\bullet}$ and 2 for $O_{(5)}$=O^{2-} respectively, depending on the strength of the $Mn_{4(a)}$–$O_{(5)}$ bond (see Figure S2 in the Supporting Information). The x-value was determined using the calculated $Mn_{4(a)}$–$O_{(5)}$ distance, $R(Mn_{4(a)}$–$O_{(5)})$, by QM and QM/MM methods. The SSB parameter was defined by Equation (1). The x value and $Mn_{4(a)}$–$O_{(5)}$ distance were in turn estimated using $R(Mn_{4(a)}$–$Mn_{3(b)})$ values by the EXAFS,[8,10] XRD,[18,30] XFEL[27–29] and computational methods.[33–47]

The $Mn_{4(a)}$–$O_{(5)}$ distances were estimated to be 2.00 and 1.82 (Å) for $O_{(5)}$=OH^- and $O_{(5)}$=O^{2-} respectively, assuming the short $Mn_{4(a)}$–$Mn_{3(b)}$ distance (2.71 Å by EXAFS[10]) of the $CaMn_4O_5$ cluster [see Eq. (3a)]. The optimized $Mn_{4(a)}$–$O_{(5)}$ distance by low-spin QM/MM under the assumption of $O_{(5)}$=O^{2-}[37,38,47] was equivalent to the latter value (1.82 Å), confirming the reliability of Equations (2) and (3a) for estimation based on the QM/MM results. The optimized $Mn_{4(a)}$–$Mn_{3(b)}$ distances obtained by QM calculations by ours and other groups[39–47] also provided 1.8~1.9 (Å) for the $Mn_{4(a)}$–$O_{(5)}$ distance in accord with the assumption of $O_{(5)}$=O^{2-} as shown in Figure 1 A. These short $Mn_{4(a)}$–$O_{(5)}$ distances in turn were considered to support the assumption of $O_{(5)}$=O^{2-} in the geometry optimizations by QM since the $Mn_{4(a)}$–$Mn_{3(b)}$ distance of EXAFS by Glöckner et al.[10] was about 2.7 Å (see Table S6). However, the observed Mn–O distances of the $CaMn_4O_5$ cluster by the EXAFS[6,7] are classified into two groups with about 1.8 and 2.0 (Å), respectively, indicating the

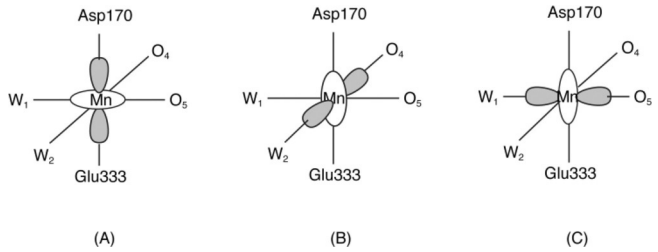

Figure 1. Three different Jahn–Teller (JT) deformation structures at the $Mn^{III}_{4(a)}$ site of the $CaMn_4O_5$ cluster in OEC of PSII by QM and QM/MM computations; A) d_{z^2} JT, B) d_{y^2} JT and C) d_{x^2} JT.

difficulty for discrimination between $R(Mn_{4(a)}–O_{(5)}) \approx 1.8$ Å and $R(Mn_{4(a)}–Mn_{3(b)}) \approx 2.7$ Å for $O_{(5)}=O^{2-}$ and $R(Mn_{4(a)}–O_{(5)}) \approx 2.0$ Å and $R(Mn_{4(a)}–Mn_{3(b)}) \approx 2.7$ Å for $O_{(5)}=OH^-$. Therefore precise determination of $R(Mn_{4(a)}–O_{(5)})$ by other experimental methods such as the low dose XRD[30] is crucial for discrimination between $O_{(5)}=O^{2-}$ and $O_{(5)}=OH^-$ in the $CaMn_4O_5$ cluster of OEC of PSII to elucidate the possibility of the X-ray damage of the XFEL[27] and SFX structures.[28,29] Furthermore, it is noteworthy that discrimination between OH^- and O^{2-} at the $O_{(5)}$ site in the S_1 state is not at all trivial because possible mechanisms for water oxidation may be different by protonation of the site.

2.3. Jahn–Teller Effect of the Mn^{III} Ion

The high-resolution XRD[18] experiment revealed that ligand fields of Mn ions are essentially octahedral in the $CaMn_4O_5$ cluster in OEC of PSII.[1,2] The first QM computation[33,34] of the S_1 structure of the $CaMn_4O_5$ cluster by 3WU2[18] elucidated the (3443) valence configuration of the $CaMn_4O_5$ cluster as mentioned above. Therefore, the Jahn–Teller (JT) effect of the $Mn^{III}_{4(a)}$ ion plays important roles for subtle deformations of the $CaMn_4O_5$ cluster.[37–39] The JT elongation axis responsible for the d_{z^2} orbital was vertical (v) to $(W_1)O–Mn^{III}_{4(a)}–O_{(5)}$ bond for the short $Mn_{4(a)}–Mn_{3(b)}$ distance (2.7 Å) as shown in Figure 1 A, suggesting the $Mn_{4(a}–O_{(5)}$ distance with about 2.0 Å for $O_{(5)}=OH^-$ or about 1.8 Å for $O_{(5)}=O^{2-}$. The intermediate $Mn_{4(a)}–Mn_{3(b)}$ distance (2.75 Å) provided the $Mn_{4(a)}–O_{(5)}$ distances with about 2.1 and 2.0 (Å) for $O_{(5)}=OH^-$ and $O_{(5)}=O^{2-}$ respectively, because the JT deformation was the d_{y^2} type, as shown in Figure 1 B. On the other hand, the JT axis for the d_{x^2} orbital becomes almost parallel to the $(W_1)O–Mn^{III}_{4(a)}–O_{(5)}$ bond, namely horizontal (h), as shown in Figure 1 C. In this case the $Mn_{4(a)}–Mn_{3(b)}$ distance is 2.80 Å for which the $Mn_{4(a)}–O_{(5)}$ distances are about 2.2 Å for both $O_{(5)}=OH^-$ and $O_{(5)}=O^{2-}$(see Figure S2 in SII.1). The horizontal JT (d_{x^2}) distortion is also operative for $R(Mn_{4(a)}–Mn_{3(b)})=$ 2.85 Å, although the $Mn_{4(a)}–O_{(5)}$ distances are about 2.3 and 2.4 (Å) for $O_{(5)}=OH^-$ and $O_{(5)}=O^{2-}$ respectively.

The estimation formula (2) and (3) are not effective for discrimination between $O_{(5)}=OH^-$ and $O_{(5)}=O^{2-}$[37–39] near the crossing region, $R(Mn_{4(a)}–O_{(5)})=2.2$ Å in Figure S2 (see Tables 1 and 5). The $Mn_{3(b}–O_{(5)}$ distance can be employed as second JT deformation index in the region. Thus, the orbital degree of freedom at the $Mn_{3(b)}$ site is one of the important factors for subtle geometrical deformation of the $CaMn_4O_5$ cluster that is regarded as a characteristic property of strongly correlated electron system (SCES).[35,39,45]

3. Theoretical Studies on the Low-Dose XRD Structures of the $CaMn_4O_5$ Cluster

3.1. Structural Symmetry Breaking of the Low-Dose XRD Structures

After the discovery[18] of the high resolution XRD structure of the $CaMn_4O_5$ cluster in OEC of PSII, X-ray damage[6,7] of the

Table 1. The Mn_4–Mn_3 distances [Å] of the $CaMn_4O_5$ cluster in the S_1 state of OEC of PSII by the low-dose (LD) XRD[30] and the estimation procedure [Eqs. (2) and (3)].

Structures	Mn_4–Mn_3 XRD	Mn_4–Mn_3[a] (Estimation)	Mn_4–$O_{(5)}$[b] Exp.(Est.)	Mn_3–$O_{(5)}$[c] Exp.	$O_{(5)}$[d]	SSB[e]	Topology[f]
5B5EA	2.82	(2.83)[a1]	2.24	2.09	$O_{(5)}=OH^-$	0.29	C_R
		(2.82)[a2]	2.24	2.09	$O_{(5)}=O^{2-}$	0.29	C_R
	2.82		(2.22)[b1]	(2.0)[c1]	$O_{(5)}=OH^-$	0.31	C_R
	2.82		(2.26)[b2]	(1.8)[c2]	$O_{(5)}=O^{2-}$	0.27	C_R
5B5EB	2.75	(2.79)[a1]	2.17	2.07	$O_{(5)}=OH^-$	0.36	R
		(2.80)[a2]	2.17	2.07	$O_{(5)}=O^{2-}$	0.36	R
	2.75		(2.08)[b1]	(2.0)[c1]	$O_{(5)}=OH^-$	0.45	R
	2.75		(1.98)[b2]	(1.8)[c2]	$O_{(5)}=O^{2-}$	0.55	R
5B66A	2.85	(2.85)[a1]	2.28	2.14	$O_{(5)}=OH^-$	0.25	C_R
		(2.83)[a2]	2.28	2.14	$O_{(5)}=O^{2-}$	0.25	C_R
	2.85		(2.28)[b1]	(2.0)[c1]	$O_{(5)}=OH^-$	0.25	C_R
	2.85		(2.38)[b2]	(1.8)[c2]	$O_{(5)}=O^{2-}$	0.15	C_R
5B66B	2.77	(2.77)[a1]	2.12	2.02	$O_{(5)}=OH^-$	0.41	R
		(2.78)[a2]	2.12	2.02	$O_{(5)}=O^{2-}$	0.41	R
	2.77		(2.12)[b1]	(2.0)[c1]	$O_{(5)}=OH^-$	0.41	R
	2.77		(2.06)[b2]	(1.8)[c2]	$O_{(5)}=O^{2-}$	0.47	R

[a] The $Mn_{4(a)}–Mn_{3(b)}$ distances were estimated by using the experimental $Mn_{4(a)}–O_{(5)}$ distance in Equation (2) and (3) under the assumption of a1) $O_{(5)}=OH^-$ and a2) O^{2-}. [b] The $Mn_{4(a)}–O_{(5)}$ distances were estimated by using the experimental $Mn_{4(a)}–Mn_{3(b)}$ distance in Equation (2) and (3) under the assumption of b1) $O_{(5)}=OH^-$ and b2) O^{2-}. [c] The $Mn_{3(b)}–O_{(5)}$ distances were estimated to be 2.0 and 1.8 for c1) $O_{(5)}=OH^-$ and c2) O^{2-}, respectively. [d] Assignment of the $O_{(5)}$ site. [e] Structural symmetry breaking (SSB) parameter. [f] Topology.

high-valent Mn^{IV} ions under the high dose conditions such as 0.43 MGy[18] was pointed out by several groups.[40–47] Tanaka et al.[30] recently performed the XRD experiments using low-doses of 0.03 (5B5EA(B)) and 0.12 MGy (5B66A(B)) for OEC of PSII. Therefore, the S_1 structure by their XRD experiments is considered to be almost X-ray-damage free (1 ~ 3 %). Table 1 summarizes the observed and calculated $Mn_{4(a)}$–$Mn_{3(b)}$ and $Mn_{4(a)}$–$O_{(5)}$ distances and SSB parameters for the low dose XRD structures.[30] From Table 1, the δ-values were 0.29 and 0.25 (Å) respectively, for A-monomers of 5B5E and 5B66,[30] exhibiting the C_R structure in our terminology (see Figure S1).[35–39] On the other hand, the δ-values were 0.36 and 0.41 for 5B5EB and 5B66B respectively, showing the R-opened (R) structure near C_R. The SSB for the B-monomers were a little larger than those of the A-monomers in the low dose XRD structure.[30] However, the δ-values of the B-monomers were only one half of the optimized value (about 0.7) of the $CaMn_4O_5$ cluster by QM and QM/MM under the assumptions of $O_{(5)}$=O^{2-} and the vertical JT (d_{z^2}) distortion (Figure 1 A).[36,38] Thus, the δ-values of the low dose XRD structures[30] are rather consistent with those of the damage-free XFEL structures[27] in contradiction to the claim based on the R-structure (Figure 1 A).[44,46]

The 5B5EA structure by low dose XRD in Figure 2 A(C) indicated that the $Mn_{3(b)}$–$Mn_{4(a)}$, $Mn_{2(c)}$–$Mn_{3(b)}$, $Mn_{1(d)}$–$Mn_{2(c)}$, $Mn_{1(d)}$–$Mn_{3(b)}$ and $Mn_{1(d)}$–$Mn_{4(a)}$ distances were 2.82(2.85), 2.76(2.78), 2.74(2.72), 3.22(3.22) and 4.91(4.92) (Å) respectively, where the corresponding values for 5B66A structure[30] (see also Figure 1 C) are given in parentheses. The observed Mn–Mn distances for A monomers indicated the following trend [Eq. (4a)]:

$$R(Mn_1-Mn_2) < R(Mn_2-Mn_3) < R(Mn_3-Mn_4) < R(Mn_1-Mn_3) < R(Mn_1-Mn_4). \quad (4a)$$

The trend, $R(Mn_2-Mn_3) < R(Mn_3-Mn_4)$, was also observed for 3WU2[18] and XFEL[27] structures.

On the other hand, the corresponding Mn–Mn distances were 2.75(2.77), 2.77(2.82), 2.65(2.72), 3.22(3.24) and 4.88(4.89) (Å) respectively, for the 5B5EB (5B66B) structures as shown in Figure 2 B(D), showing a different trend [Eq. (4b)]:

$$R(Mn_1-Mn_2) < R(Mn_3-Mn_4) < R(Mn_2-Mn_3) < R(Mn_1-Mn_3) < R(Mn_1-Mn_4) \quad (4b)$$

The reverse trend, $R(Mn_3-Mn_4) < R(Mn_2-Mn_3)$, was also observed for the EXAFS structure reported by Yano and co-workers.[8,10] The average Mn–Mn distances of $Mn_{3(b)}$–$Mn_{4(a)}$, $Mn_{2(c)}$–$Mn_{3(b)}$ and $Mn_{1(d)}$–$Mn_{2(c)}$ are 2.77, 2.78, 2.72 and 2.77 (Å) respectively for 5B5EA, 5B66A, 5B5EB and 5B66B[28] in agreement with the average Mn–Mn distances revealed by the damage-free XFEL,[27] namely 2.72 Å for 4UB6, and 2.78 Å for 4UB8, and 2.73 Å for EXAFS.[8,10] Thus, there is no serious differences (namely within the experimental uncertainty) of the average Mn–Mn distance among the low dose XRD,[30] XFEL[27] and EXAFS[10] structures. On the other hand, the corresponding average Mn–Mn distances were 2.91 and 2.86 (Å) for 3WU2A and 3WU2B,[18] respectively, indicating non-negligible elongations (0.1 ~ 0.2 Å) because of the X-ray damage.[27,30,45] However, the topological structure of 3WU2 [see Eq. (4a)] is similar to

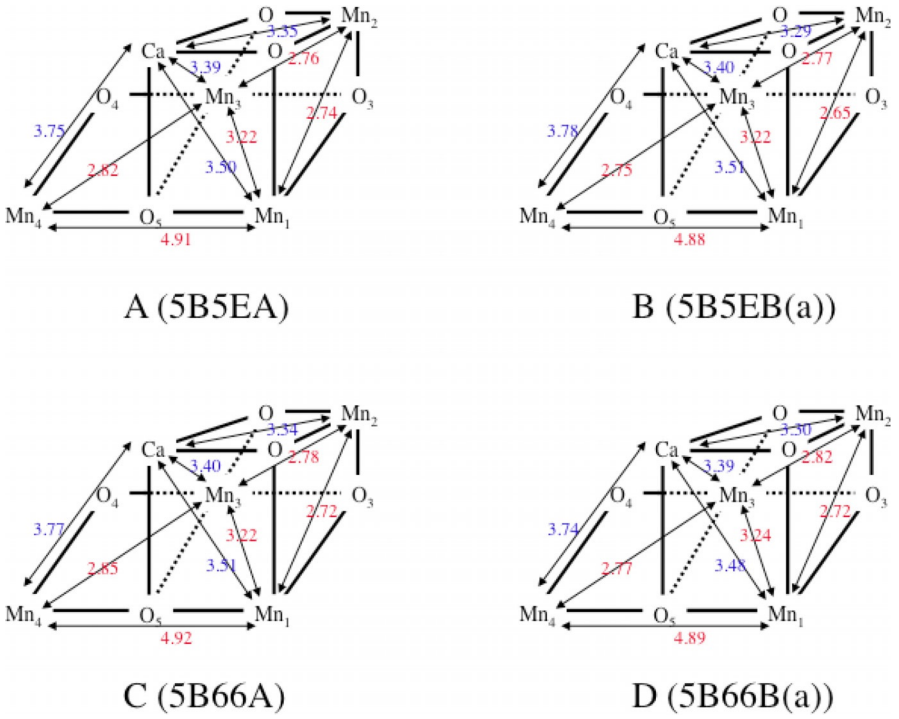

Figure 2. Three dimensional (3D) structures and Mn–Mn and Ca–Mn distances of the $CaMn_4O_5$ cluster in oxygen evolving complex (OEC) determined by an extremely low dose XRD experiment by Tanaka et al.:[28] A) 5B5EA, B) 5B5EB, C) 5B66A and D) 5B66B.

that of XFEL,[27] namely 5% reduction of the Mn–Mn distances of 3WU2[18] is necessary for production of the XFEL structure.[27]

The Ca–$Mn_{4(a)}$, Ca–$Mn_{3(b)}$, Ca–$Mn_{2(c)}$ and Ca–$Mn_{1(d)}$ distances were 3.75(3.77), 3.39(3.40), 3.35(3.34) and 3.50(3.51) (Å) respectively for 5B5EA(5B66A). The corresponding Ca–Mn distances were 3.78(3.74), 3.40(3.39), 3.29(3.30) and 3.51(3.48) respectively for 5B5EB(5B66B).

The Ca–Mn distances were not so different between A- and B-monomers of the dimer structure of OEC of PSII in both samples, indicating a general tendency referred to as the rule IIa[35–39] for the XRD[18] and XFEL[27] structures [Eq. (5)].

$$R(Ca-Mn_2) < R(Ca-Mn_3) < R(Ca-Mn_1) < R(Ca-Mn_4) \quad (5)$$

The divalent Ca^{II} ion is therefore irrelevant to the X-ray damage.

3.2. Application of the Jahn–Teller Deformation Formula to the $CaMn_4O_5$ Cluster

The JT deformation formula [see Eqs. (2) and (3)] were applied to the low dose XRD structures by Tanaka *et. al.*[30] which elucidated subtle different structures between A- and B-monomers. The observed $Mn_{4(a)}$–$O_{(5)}$ distances for 5B5EA(5B66A) were 2.24(2.28) (Å) respectively, indicating that the $Mn_{3(b)}$–$Mn_{4(a)}$ distances were estimated to be 2.83(2.85) (Å) for $O_{(5)}$=OH^- and 2.82(2.83) (Å) for $O_{(5)}$=O^{2-} respectively, in accord with the parallel JT (d_{x^2}) elongation illustrated in Figure 1C. On the other hand, the $Mn_{4(a)}$–$O_{(5)}$ distances were estimated to be 2.22(2.28) (Å) for $O_{(5)}$=OH^- and 2.26(2.38) (Å) for $O_{(5)}$=O^{2-} respectively, using the $Mn_{3(b)}$–$Mn_{4(a)}$ distances, namely 2.82 (2.85) (Å) for 5B5EA(5B66A). The Equations (2) and (3) using the $Mn_{3(b)}$–$Mn_{4(a)}$ and $Mn_{4(a)}$–$O_{(5)}$ distances were not conclusive for discrimination between $O_{(5)}$=OH^- and $O_{(5)}$=O^{2-} (except for 5B66A for which $O_{(5)}$=OH^-) near the crossing region of the JT deformation lines (see Figure S2 in SII.1). Therefore, the second criterion, namely $Mn_{3(b)}$–$O_{(5)}$ distance, was employed for the discrimination.[37–39] As shown in Table 2, the observed $Mn_{3(b)}$–$O_{(5)}$ distances by the LD XRD were 2.09 and 2.14 (Å) for 5B5EA and 5B66A respectively. These values are rather consistent with the assumption of $O_{(5)}$=OH^- in Table S1, supporting the S_1 structure by XFEL[27] and structure of A monomer of LD XRD.[30]

The JT deformation formula were also applied to the low dose XRD structures of the B-monomer.[30] The observed $Mn_{4(a)}$–$O_{(5)}$ distances for 5B5EB(5B66B) were 2.17(2.12) (Å), providing that the estimated $Mn_{3(b)}$–$Mn_{4(a)}$ distances were 2.79(2.77) (Å) for $O_{(5)}$=OH^- and 2.80(2.78) (Å) for $O_{(5)}$=O^{2-} respectively. On the other hand, the $Mn_{4(a)}$–$O_{(5)}$ distances for 5B5EB(5B66B) were estimated to be 2.08(2.12) (Å) for $O_{(5)}$=OH^- and 1.98(2.06) (Å) for $O_{(5)}$=O^{2-} respectively, using the observed $Mn_{3(b)}$–$Mn_{4(a)}$ distance, namely 2.75 (2.77) (Å) for 5B5EB(5B66B). Interestingly, the $Mn_{4(a)}$–$O_{(5)}$ distance estimated using the $Mn_{3(b)}$–$Mn_{4(a)}$ distance (2.75 Å) of 5B5EB was about 2.1 Å in agreement with the assumption of $O_{(5)}$=OH^- in Table S1. The observed $Mn_{3(b)}$–$O_{(5)}$ distance for 5B5EB was 2.07 Å, further supporting the assumption of $O_{(5)}$=OH^-. The protonation of the $O_{(5)}$ site is also consistent with the $Mn_{4(a)}$–$O_{(5)}$ distance (2.12) for 5B66B. Thus the JT distortion for the B-monomer was consistent with the JT (d_{y^2}) deformation in Figure 1B. Interestingly, the longer $Mn_{4(a)}$–$O_{(5)}$ distances of the B-monomers are rather consistent with the longer $Mn_{4(a)}$–$O_{(5)}$ distance (about 2.0 Å) by EXAFS.[6] This indicates the d_{y^2}-JT-type B-structure (see Figure 1B) for the EXAFS results[8,10] as shown in Table S6 (see the Supporting Information).

In order to confirm the above assignments, the Mn–O distances of the octahedral ligand fields for the $Mn^{III}_{4(a)}$ ion were depicted in Figure 3. The observed $Mn_{4(a)}$–$O_{(5)}$ and $Mn_{4(a)}$–O(W1) distances for 5B5EA(5B66A) were 2.24(2.28) and 2.19(2.19) (Å) respectively, as shown in Figure 3A(D), indicating the parallel JT elongation (d_{x^2}) illustrated in Figure 1C. The observed $Mn_{4(a)}$–$O_{(5)}$ and $Mn_{4(a)}$–O(W1) distances for 5B5EB(5B66B) were 2.17(2.12) and 2.10(2.10) (Å) respectively, as shown in Figure 3B(E), showing the shortening of 0.07(0.16) and 0.09(0.09) as compared with those of 5B5EA(5B66A). On the other hand,

Table 2. The $Mn_{4(a)}$–$O_{(5)}$ and $Mn_{3(b)}$–$O_{(5)}$ distances [Å] of the $CaMn_4O_5$ cluster in the S_1 state of OEC of PSII based on the estimation procedure using the Mn_4–Mn_3 distance [Å] obtained by the mixing of the $S_1(C_R)$ and $S_0(C_L)$ structures [Eq. (7)].

Structures[a]	Mn_4–Mn_3	$\alpha(C_L)$ [%][b]	Mn_4=$O_{(5)}$[c]	Mn_3–$O_{(5)}$[d]	SSB[e]	Topology[f]
$S_1(C_R)$	2.80	0.0	2.18	2.00	0.35	R
	2.81	3.3	2.20	2.01	0.33	R
	2.82	6.7	2.22	2.03	0.31	C_R
	2.83	10.0	2.24	2.04	0.29	C_R
	2.84	13.3	2.26	2.05	0.27	C_R
$(1-\alpha)$ $S_1(C_R)$	2.85	16.7	2.28	2.07	0.25	C_R
$+\ \alpha$ $S_0(C_L)$	2.86	20.0	2.30	2.08	0.23	C_R
	2.87	23.3	2.32	2.09	0.21	C_R
	2.88	26.7	2.34	2.11	0.19	C_R
	2.89	30.0	2.36	2.12	0.17	C_R
	2.90	33.3	2.38	2.13	0.15	C_R
	2.91	36.7	2.40	2.15	0.13	C_R
	2.92	40.0	2.42	2.16	0.11	C_R

[a] The geometrical parameters are given by the mixing of the $S_1(C_R)$ and $S_0(C_L)$ structures. [b] The mixing ratio $\alpha(C_L)$ for the C_R structure. [c] The $Mn_{4(a)}$–$O_{(5)}$ distance for the $(1-\alpha)S_1(C_R) + \alpha S_0(C_L)$ structure. [d] The $Mn_{3(b)}$–$O_{(5)}$ distance for the mixed $(1-\alpha)$ $S_1(C_R) + \alpha$ $S_0(C_L)$ structure. [e] Structural symmetry breaking (SSB) parameter. [f] The right-opened structure (R).

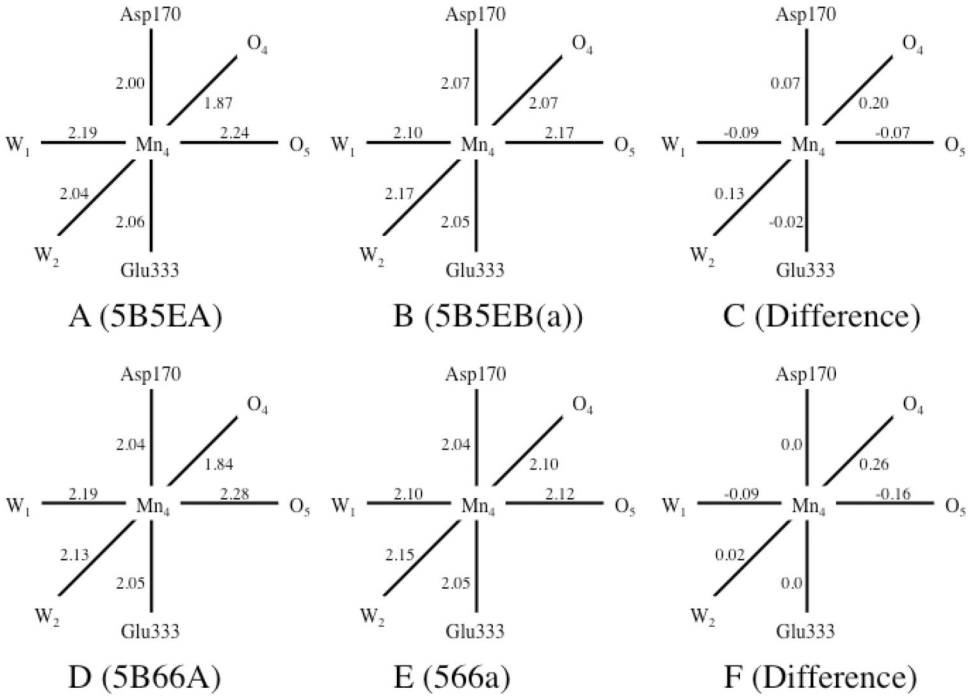

Figure 3. Schematic illustration of the Mn–O bond lengths in the octahedral ligand field of the $Mn_{4(a)}$ ion in the $CaMn_4O_5$ cluster in OEC for A) 5B5EA, B) 5B5EB(a), D) 5B66A and E) 5E66B(a). Differences of the Mn–O distances between the A and B(a) monomers in 5B5E and 5B66 are shown in (C) and (F), respectively.

the $Mn_{4(a)}$–$O_{(4)}$ and $Mn_{4(a)}$–O(W2) distances for 5B5EA(5B66A) were 1.87(1.84) and 2.04(2.13) (Å), respectively, as shown in Figure 3 A(D). The corresponding values for 5B5EB(5B66B) are 2.07(2.10) and 2.17(2.15) (Å) as shown in Figure 3 B(E), indicating the elongations of 0.20(0.26) and 0.13(0.02) (Å) respectively, as shown in Figure 3 C(F) in accord with the JT (d_{y^2}) deformation. Therefore, 5B5EB(5B66B) are regarded as a JT (d_{y^2}) deformed structure in Figure 1 B, also suggesting that the EXAFS structure[8, 10] with the different topology [see Eq. (4b)] may be explained with the B-structure by the LD XRD.[30] The LD XRD structures with no significant X-ray damage[30] was not consistent with the R-structure with the JT (d_{z^2}) distortion in Figure 1 A, where the $Mn_{3(b)}$–$Mn_{4(a)}$ and $Mn_{4(a)}$–$O_{(5)}$(=O^{2-}) distances are estimated to be about 2.7 and 1.8 (Å), respectively.

3.3. Importance of the $Mn_{3(b)}$–$O_{(5)}$ Distances in the $CaMn_4O_5$ Cluster

The discrimination between O^{2-} and OH^- at the $O_{(5)}$ site is hardly possible based on the JT deformation formula in the region of the R($Mn_{4(a)}$–$O_{(5)}$) = 2.2 Å (see Figure S2). In this situation, the $Mn_{3(b)}$–$O_{(5)}$ bond lengths become an important JT deformation index for discrimination between O^{2-} and OH^- at the $O_{(5)}$ site of the $CaMn_4O_5$ cluster. The $Mn^{IV}{}_{3(b)}$–$O_{(5)}$ bond lengths are usually about 1.8 ~ 1.9 Å for $O_{(5)}$=O^{2-} because of no JT effect of Mn^{IV} ion, as shown previously (see Tables 5 and S5).[39] The $Mn^{IV}{}_{3(b)}$–$O_{(5)}$H bond length after protonation of the $O_{(5)}$ site is 2.0 ~ 2.1 (Å) because of no JT effect. On the other hand, the $Mn^{III}{}_{3(b)}$–$O_{(5)}$H bond length may be elongated to 2.3 ~ 2.4 Å if the JT elongation axis is parallel to the $HO_{(5)}$–$Mn_{b(3)}$–O(Glu 354) bond in the $CaMn_4O_5$ cluster. In fact, $Mn_{3(b)}$–$O_{(5)}$ bond length by 3WU2 structure[18] was 2.4 Å because of the reduction of $Mn^{IV}{}_{3(b)}$ into $Mn^{III}{}_{3(b)}$.[30] Thus, the JT deformation formula revealed by the computational results[35–39] and available experiments for Mn complexes provide guiding principles for understanding of variations of Mn–O bond lengths of the $CaMn_4O_5$ cluster of OEC of PSII.

Nevertheless, several theoretical papers[41,42,44,46] suggested the possibility of the radiation damage of the XFEL structure.[27] Previously[39] we have estimated the fraction of the S_0 component in the observed XFEL structure[27] on the basis of the following equation under the assumption of 2.0 and 2.4 (Å) for the $Mn_{3(b)}$–$O_{(5)}$ distances of the C_R structures in the S_1 and S_0 states, respectively [Eq. (6)]:

$$\begin{aligned} R(Mn_{3(b)}-O_{(5)}) &= (1-\alpha)R(Mn^{IV}{}_{3(b)}-OH_{(5)}) = 2.0\,\text{for}\,S_1(C_R) \\ &+\alpha R(Mn^{III}{}_{3(b)}-OH_{(5)}) = 2.4\,\text{for}\,S_0(C_R)) \end{aligned} \quad (6)$$

where the C_R structures are used for both S_1 and S_0 states. Here the Equation (6) was applied for the low dose XRD structures.[30] The weight (α) of the S_0 component was estimated to be 17.5 and 35 (%) respectively for 5B5EA and 5B66A structures. The estimated contribution of the $S_0(C_R)$ component for 5B5EA is smaller than the estimated value (25 %) for the no pre-flash experiment, whereas it seems non negligible for 5B66A structure[46] under the assumption of no experimental uncertainty. However, the contamination of the $S_0(C_R)$ structure in 5B66A resulted in a very small elongation (2.85–2.82 = 0.03 Å) of the $Mn_{3(b)}$–$Mn_{4(a)}$ distance because of the same C_R topology. Therefore, the observed structure of the A monomer by the LD XRD experiment[30] is fully compatible with the

damage-free XFEL structure,[27] particularly 4UB6 structure and reassigned EXAFS structure[39] (see Table S6).

The estimated fractions (α) of the $S_0(C_R)$ component by Equation (6) were 22 and 5 (%) respectively, for 5B5EB and 5B66B structures.[30] The estimated contribution of the S_0 structure for 5B5EB is smaller than 25%, whereas it seems negligible for 5B66B structure for which the observed $Mn_{3(b)}$—$O_{(5)}$ distance is 2.02 Å. Therefore, the observed structure of the B monomer by the low dose (LD) XRD experiment[30] is fully compatible with the JT (d_{y^2}) deformed structure in Figure 1B instead of the JT (d_{z^2}) structure in Figure 1A. Thus, the nature of the chemical bonds of the $CaMn_4O_5$ cluster of OEC is labile,[33] indicating the structural deformations (see Figure 4).

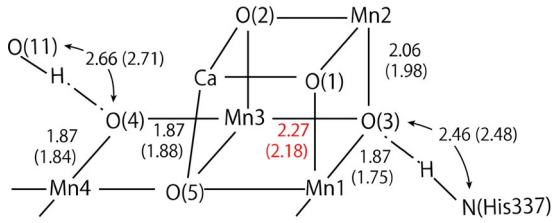

(A)

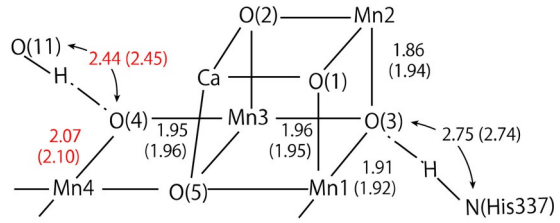

(B)

Figure 4. The Mn–O distances and hydrogen bonding interactions in the dimer of OEC of PSII by low-dose XRD experiments.[28] A) A-monomers by 5B5EA(5B66A) and B) B-monomers of 5B5EB(5B66B).

3.4. Estimation of Radiation Damage by the $Mn_{3(b)}$—$Mn_{4(a)}$ Distances in the $CaMn_4O_5$ Cluster

The pre-flash procedure for generation of the pure S_1 state was not performed for the LD XRD experiments,[30] indicating a possibility of the contamination of the S_0 component. The JT deformation formula indicate that the $Mn_{3(b)}$—$Mn_{4(a)}$ distances can be used for estimation of the possible fraction of the S_0 component, under the assumption of reduction of the high-valent $Mn^{IV}{}_{3(b)}$ ion into $Mn^{III}{}_{3(b)}$ as follows [Eq. (7)]:

$$R(Mn_{3(b)}-Mn_{4(a)}) = (1-\alpha)R(Mn_{3(b)}-Mn_{4(a)} = 2.80)\ \text{for}\ S_1(C_R) + \alpha R(Mn_{3(b)}-Mn_{4(a)} = 3.10)\ \text{for}\ S_0(C_L) \quad (7)$$

where the C_L structure for the S_0(3343) state was employed for estimation. The mixing coefficient (α) are summarized in Table 2. The α-values are 6.7 and 16.7 (%) respectively, for 5B5EA and 5B66A for which the $Mn_{3(b)}$—$Mn_{4(a)}$ distances are 2.82 and 2.85 (Å) respectively. Therefore, the S_0 components for the A-monomers are smaller than 25%, showing the normal behavior. The $Mn_{4(a)}$—$O_{(5)}$ distances estimated by the α-values are 2.22(2.24) and 2.28(2.28) (Å) respectively, where the observed distances are given in parentheses. The estimated (observed) $Mn_{3(b)}$—$O_{(5)}$ distances are 2.03(2.09) and 2.07(2.14) (Å), respectively. The JT deformation formulae [see Eqs. (2) and (3)] work well for examination of the S_0 contamination for the LD XRD structures.[30] The A-monomer by the LD XRD[30] is essentially regarded as the $S_1(C_R)$ structure even if the partial $S_0(C_L)$ contamination is taken into account.

We have assumed the reduction of the high-valent $Mn^{IV}{}_{3(b)}$ into the $Mn^{III}{}_{3(b)}$ ion in the S_1 to S_0 transition in Equation (7). However, the reduction of $Mn^{III}{}_{4(a)}$ into $Mn^{II}{}_{4(a)}$ by chemical origins[45] is also conceivable, yielding the S_0 state with the (2443) valence configuration.[36] The optimized $Mn_{3(b)}$—$Mn_{4(a)}$, $Mn_{2(c)}$—$Mn_{3(b)}$, $Mn_{1(d)}$—$Mn_{2(c)}$, $Mn_{1(d)}$—$Mn_{3(b)}$ and $Mn_{4(a)}$—$O_{(5)}$ distances were 2.97, 2.81, 2.75, 3.32 and 2.44 (Å) respectively for the $S_0(C_R)'$ state with the (2443) configuration.[36] Therefore the $Mn_{3(b)}$—$Mn_{4(a)}$ distances are also estimated as follows [Eq. (8)]:

$$R(Mn_{3(b)}-Mn_{4(a)}) = (1-\alpha)R(Mn_{3(b)}-Mn_{4(a)} = 2.80)\ \text{for}\ S_1(C_R) + \alpha R(Mn_{3(b)}-Mn_{4(a)} = 2.97)\ \text{for}\ S_0(C_R)'. \quad (8)$$

The α-values calculated by using $R(Mn_{3(b)}$—$Mn_{4(a)})$ distance of $S_0(C_R)'$ are 11.8 and 29.4 (%), respectively. Therefore the estimated $Mn_{4(a)}$—$O_{(5)}$ distances for 5B5EA and 5B66A are 2.21(2.24) and 2.26(2.28) (Å) respectively, where the observed distances are given in parentheses. The main component of the A-monomer[30] based on the $Mn_{3(b)}$—$Mn_{4(a)}$ and $Mn_{4(a)}$—$O_{(5)}$ distances is regarded as the $S_1(C_R)$ structure in Figure 1C.

Several theoretical papers[44,46] claimed that the "damage-free" XFEL structure[27] may be regarded as the S_0 structure. The α-values by Equation (7) assuming the mixing of the $S_0(C_R)$(3343) configuration are 20, 10, 27 and 37 (%) respectively for 4UB6A(2.86 Å), 4UB6a(2.83 Å), 4UB8A(2.88 Å) and 4UB8a(2.91 Å)[27] for which the observed $Mn_{3(b)}$—$Mn_{4(a)}$ distances are given in parentheses. On the other hand, the corresponding α-values by Equation (8) assuming the mixing of the $S_0(C_R)'$(2443) configuration are 35 (92), 18 (62), 47(77) and 65 (67) (%) respectively, where the corresponding values estimated by the EXAFS line simulations using 2.83, 2.86, 2.83 and 2.88 (Å) for $R(Mn_{3(b)}$—$Mn_{4(a)})$ respectively, are given in parentheses.[46] High(HO)- and low(LO)-oxidation paradigms[2,47] have been proposed for the valence state of the $CaMn_4O_5$ cluster in OEC of PSII (see Ref. [47] and section SV in the Supporting Information). According to the HO and LO paradigms,[2,47] Mn^{III} and Mn^{II} ions are involved in the S_0 state, respectively. The Equation (7), consistent with the HO paradigm, suggests that the fraction of the S_0-component for 4UB6 is normal for the no pre-flash experiment,[27] whereas the estimated value for 4UB8a suggests the non-negligible uncertainty.[44,46] 4UB6 is also acceptable for the Equation (8) for the LO paradigm.[47] Therefore, our conclusion is different from the assumption of the better quality of 4UB8 than that of 4UB6 employed for the electron

Table 3. The spin densities on the $Mn_{1(d)}$, $Mn_{2(c)}$, $Mn_{3(b)}$, $Mn_{4(a)}$ and $O_{(4)}$ ions of the XFEL structures[27] of the $CaMn_4O_5$ cluster of OEC of PSII by UB3LYP method.[48]

Sites	Case I 4UB6A	(X = O^{2-}, 4UB6a	Y = H_2O) 4UB8A	4UB8a	Case II 4UB6A	(X = OH^-, 4UB6a	Y = OH^-) 4UB8A	4UB8A
Mn4	4.23 (3.86)[a]	4.29 (3.89)[a]	4.34 (3.96)[a]	4.29 (3.95)[a]	4.07 (3.93)[a]	4.04 (3.96)[a]	4.14 (4.05)[a]	4.12 (4.06)[a]
Mn3	3.33	3.14	3.68	3.60	3.21	3.11	3.68	3.60
Mn2	3.12	2.88	3.18	3.07	3.11	2.88	3.18	3.07
Mn1	3.78	3.75	3.73	3.70	3.79	3.76	3.73	3.69
$O_{(4)}$	−0.37	−0.40	−0.41	−0.34	−0.14	−0.08	−0.09	−0.06

[a] The renormalized spin density $Q_R = Q(Mn_4) + Q(O_{(4)})$ to remove the internal reduction of Mn ion by the spin polarization of the Mn_4–$O_{(4)}$ bond is given in parentheses.

density maps analysis by Wang et al.,[46] which predicted 100, 88, 77 and 78 (%) S_1 to S_0 reductions for 4UB6A, 4UB6B, 4UB8A and 4UB8B respectively. The LO paradigm reported by Petrie et al.[47] provided different explanations of the XRD structure[18] as described in the Supporting Information, Section SV.

The spin densities (Q) on the Mn_1, Mn_4 and $O_{(4)}$ atoms are another chemical index[37,39] for elucidation of the reduction of the Mn^{III} and Mn^{IV} ions, for which the Q values are about 4.0 and 3.0 respectively. Table 3 summarizes the calculated Q values by the QM (UB3LYP) method.[48] The spin densities on the $Mn_{4(a)}$ are in the range; 4.23 ~ 4.37, indicating the internal reduction by the spin polarization (SP) of the $Mn_{4(a)}$–$O_{(4)}$ bond under the assumption of W2 = H_2O and $O_{(5)}$ = O^{2-}. Therefore, the renormalized spin densities (Q_R) are obtained by using the negative spin densities on the $O_{(4)}$ atom (see Table 3). The Q values for the $Mn_{4(a)}$ ion are about 4.0, indicating the Mn^{III} valence state. The SP effect for the $Mn_{4(a)}$-$O_{(4)}$ bond is small for the case; W2 = $O_{(5)}$ = OH^-, indicating Q ≈ 4.0 on $Mn_{4(a)}$. The spin densities (Q) on the $Mn_{1(d)}$ ion are also 3.7 ~ 3.8 in agreement with the Mn^{III} valence state. The Q-values on the $Mn_{2(c)}$ ion are 2.9 ~ 3.2 in compatible with the Mn^{IV} valence state. On the other hand, spin densities (Q) on the $Mn_{3(b)}$ ion are 3.21, 3.11, 3.49 and 3.64, respectively, for 4UB6A, 4UB6B, 4UB8A and 4UB8B. The spin densities of the $Mn_{3(b)}$ site for 4UB8 were significantly larger than 3.0, suggesting that non-negligible reduction of the $Mn^{IV}{}_{3(b)}$ into $Mn^{III}{}_{3(b)}$, namely, the mixing of $S_0(C_R)$(3343) under the assumption of no experimental uncertainty. Present and previous[39] computational results indicate that the XFEL structure (4UB6) by Suga et al.[27] corresponds to the S_1 structure against the claim by other groups[44,46] and it is compatible with the structure of A monomer by LD XRD.[30] Young et al. also used the XFEL structure[27] for analysis of the new SFX results (5KAF)[29] for dark stable state.

4. Discussion

4.1. Examination of the Right-Opened structure in the S_1 State

The structures of A-monomers with R($Mn_{3(b)}$–$Mn_{4(a)}$) > 2.8 Å by the LD XRD[30] are compatible with the XFEL structures[30] and the re-assigned EXAFS structure (see Table S6).[37–39] On the other hand, the $Mn_{3(b)}$–$Mn_{4(a)}$ distances of 5B5EB and 5B66B[30] are shorter than 2.80 Å, suggesting that the geometrical structures of B-monomers may be explained by mixing of the right-opened (R) S_1 structure (see Figure 1 A) with the slightly right (C_R)- and left (C_L)-elongated quasi-central S_0 structures (see Figure S1) as follows (X = R or L) [Eq. (9)]:

$$\begin{aligned} R(Mn_{3(b)}-Mn_{4(a)}) = (1-\alpha)R(Mn_{3(b}-Mn_{4(a)} = 2.70)\,\text{for}\,S_1(R) \\ +\alpha R(Mn_{3(b)}-Mn_{4(a)} = R_{cal})\,\text{for}\,S_0(C_X)) \end{aligned} \quad (9)$$

where R_{cal} are 2.80 and 3.10 (Å) for $S_0(C_R)$ and $S_0(C_L)$ respectively. Table S2 summarizes the mixing coefficients (α) and estimated $Mn_{4(a)}$–$O_{(5)}$ and $Mn_{3(b)}$–$O_{(5)}$ distances. From Table S2 (see SII.2), the $Mn_{4(a)}$–$O_{(5)}$ distances for the mixed structures are estimated to be in the range; 1.82 ≈ 1.90 (Å) under the assumptions of R($Mn_{3(b)}$–$Mn_{4(a)}$) = 2.71 ~ 2.74 (Å).

The α-values calculated by using R($Mn_{3(b)}$–$Mn_{4(a)}$) = 2.75 Å for 5B5EB are 25 and 12.5 (%), respectively, for the $S_0(C_R)$ and $S_0(C_L)$ mixings into the S_1(R) structure, indicating that the $S_1(R)$-structure is acceptable for 5B5EB. However, the calculated $Mn_{4(a)}$–$O_{(5)}$ distance is 1.93 Å for both mixing cases, and in contradiction to the observed value of 2.17 Å. The calculated $Mn_{3(b}$–$O_{(5)}$ distances are 1.95 and 1.88 Å, respectively, for the $S_0(C_R)$ and $S_0(C_L)$ mixings, but the observed value is 2.07 Å. Therefore the observed $Mn_{4(a)}$–$O_{(5)}$ and $Mn_{3(b)}$–$O_{(5)}$ distances for 5B5EB are hardly explained by the mixing in Equation (9) based on the Mn–Mn distances.

The α-values for 5B66B with R($Mn_{3(b)}$–$Mn_{4(a)}$) = 2.77 Å[30] are calculated to be 35 and 17.5 (%) respectively, for the $S_0(C_R)$ and $S_0(C_L)$ mixings into the S_1(R) structure, indicating that the former value for the $S_0(C_R)$ mixing is over the normal value (25 %). On the other hand, the latter value for the $S_0(C_L)$ mixing is normal, indicating that the S_1(R)-structure in Figure 1 A seems feasible for 5B66B. The calculated $Mn_{4(a)}$–$O_{(5)}$ and $Mn_{3(b)}$–$O_{(5)}$ distances for the latter mixing are 1.99(2.12) and 1.91(2.02) (Å) respectively, where the corresponding observed values are given in parentheses (see Section SII in the Supporting Information). The high-resolution LD XRD structure with experimental uncertainty smaller than 0.1 Å is desirable for further discussion of the S_1(R) structure in Figure 1 A.

The mixing for S_1(R) with $S_0(C_R)'$ is also conceivable as follows [Eq. (10)]:

$$R(Mn_{3(b}-Mn_{4(a)}) = (1-\alpha)R(Mn_{3(b)}-Mn_{4(a)} = 2.70)\ \text{for}\ S_1(R) + \alpha R(Mn_{3(b}-Mn_{4(a)} = 2.97)\ \text{for}\ S_0(C_R)'. \quad (10)$$

The estimated α-values are 18.5 and 25.9 (%) respectively, for 5B5EB and 5B66B, indicating that the d_{z^2}-JT type R-structure seems acceptable. However, the elongated $Mn_{4(a)}$–$O_{(5)}$ distances for 5B5EB and 5B66B are estimated to be 1.90 (2.17) and 1.95(2.12) (Å) respectively, where the corresponding observed values are given in parentheses. Therefore the observed $Mn_{4(a)}$–$O_{(5)}$ and $Mn_{3(b}$–$O_{(5)}$ distances for 5B5EB are hardly explained by the mixing in Equation (10).

The valence configuration of the $Mn_{3(b)}$ site should be smaller than the formal Mn^{IV} (Q = 3.0) of the pure S_1 configuration if the $S_0(C_R)$ or $S_0(C_L)$ with the (3343) configuration were mixed in the LD XRD structure without the pre-flash (see Table 3). On the other hand, the valence configuration of the $Mn_{4(a)}$ site should be smaller than the formal Mn^{III}(Q = 4.0) with mixing of the $S_0(C_R)'$ with the (2443) configuration. Therefore, precise determination of the valence state of each Mn ion in the LD XRD structures by the X-ray spectroscopy is desirable for discrimination between the mixing schemes (9) and (10) on the experimental ground.[2] The HO and LO paradigms[2,47] relating to valence states of Mn ions are discussed in the Supporting Information, Section SV.

4.2. X-ray Induced Atomic Displacements by XFEL

Several experimental and theoretical studies[49–52] on X-ray-induced atomic displacements within the XFEL pulse durations have been performed in relation to X-ray damages of serial femtosecond crystallography (SFX) (see SIII). Nagaya et al.[49,50] investigated the electronic and nuclear dynamics of I-containing organic molecules such as 5-iodouracil (5-IU) induced by intense hard X-ray pulses at the XFEL facility (SACLA), elucidating that the changes of C–O, C–N and C–C distances of 5-IU were less than several % at the 10 fs pulse duration, and in contrast, the I–C length of 5-IU did not change in 30 fs. Amin et al.[51,52] performed ab initio molecular dynamics simulation of OEC, where the nuclei move classically in a full quantum potential created by electron density under the effect of strong laser pulse in the Ehrenfest dynamics regime (see details SIII). The computational results[51,52] showed that the Mn-Mn and Mn-Ca distances were less affected by radiation damage due to their heavy masses, while the $O_{(5)}$ atom moved significantly. The $Mn_{4(a)}$–$Mn_{3(b)}$ (Ca–$O_{(5)}$) distances for the S_1 structure (see Figure 1 A) were calculated to be 2.89(2.47), 2.90(2.47) and 3.08(2.53) (Å) respectively, after 0, 10 and 50 fs duration of the XFEL pulse.[51,52] Therefore, the elongations by X-ray damage were 0.01(0.00) and 0.19(0.06) (Å) for 10 and 50 fs irradiations, respectively. The calculated $Mn_{4(a)}$–$O_{(5)}$ ($Mn_{3(b}$–$O_{(5)}$) distances[51,52] for the S_1 structure were 1.88(1.87), 1.92(1.89) and 2.34(2.01) (Å) respectively, after 0, 10 and 50 fs irradiation of XFEL. The elongations by X-ray damage were 0.04(0.02) and 0.46(0.14) (Å) for 10 and 50 fs irradiations, respectively, indicating the 2.13(1.07) and 24.4 (7.49) % elongations. The $Mn^{III}{}_{4(a)}$–$O_{(5)}$ bond was sensitive to the radiation damage as compared with the $Mn^{IV}{}_{3(b)}$–$O_{(5)}$ bond.

According to the above computational results,[51,52] the $Mn^{III}{}_{4(a)}$–$O_{(5)}$ bond lengths of the XFEL structures[27] were estimated using the Coulomb explosion distance (Δ_{XFEL}) as follows [Eq. (11)]:

$$R(Mn_{4(a)}-O_5)_{correct.} = R(Mn_{4(a)}-O_5)_{XFEL} - \Delta_{XFEL} \quad (11)$$

where Δ_{XFEL} were given by the above 2.13 (10 fs) and 24.4 (50 fs) % elongations of the $Mn_{4(a)}$–O_5 distance of XFEL structures.[27] The 5 and 10 (%) elongations were also examined for weak and medium explosions, respectively. Table 4 summarizes the calculated $Mn_{4(a)}$–O_5 distances, for which the $Mn_{4(a)}$–$Mn_{3(b)}$ distances are estimated using Equation (3). The explosion distances (Δ_{XFEL}) were about 0.05, 0.1, 0.2 and 0.6 (Å) respectively, for 2.13 (10 fs), 5 (a fs), 10 (b fs) and 24.4 (50 fs) % elongations, where $10 < a < b < 50$. The slightly elongated $Mn_{4(a}$–O_5 distances (about 2.3 Å) of the XFEL structures at 10 fs pulse duration (SACLA)[27] are shortened by about 0.05 ~ 0.1 Å, and the corrected $Mn_{4(a)}$–O_5 distances by Equation (11) are therefore compatible with those of the A-monomers of the LD XRD structure.[30] On the other hand, the corrected $Mn_{4(a)}$–O_5 distances for the medium (10 %) and long (50 fs) pulse durations are formally compatible with the $Mn_{4(a)}$–O_5 distances of the B-monomers of the LD XRD[30] and R-structures in Figure 1 A, respectively. The computational results suggest that the atomic displacement of the $Mn^{III}{}_{4(a)}$–$O_{(5)}$ bond of the $CaMn_4O_5$ cluster by XFEL[27] is small (< 0.1 Å) because of the short pulse width (10 fs) at SACLA.[53] The situation is the same for the $Mn^{III}{}_{3(b)}$–$O_{(5)}$ bond (see Table S5). The high-resolution XFEL (~40 fs) structure at LCLS[29] is really desirable for comparison (see SIII).

4.3. Comparisons Between Low-Dose XRD and New SFX Structures

The d_{y^2}-JT type structures (see Figure 1 B) of B-monomers by LD XRD[30] were in agreement with the EXAFS structure with the {2, 1, 0} Mn-Mn distances[10] under the assumption of protonation of the $O_{(5)}$ site ($O_{(5)}$=OH^-). Detailed discussions on the EXAFS results[2,3] relating to LD XRD[30] were given in Section SIV in the Supporting Information.[39] Here the JT deformation Equations (1)–(3) applied for the analysis of very recent SFX structures with and without preflash in the dark stable state reported by Suga et al.[28] and Young et al.[29]. Table 5 summarizes the observed and calculated $Mn_{4(a)}$–$Mn_{3(b)}$ and $Mn_{4(a)}$–$O_{(5)}$ distances and SSB parameters for these SFX structures. From Table 5, the SFX results for A-monomer of 5GTH without preflash[28] elucidated that the $Mn_{4(a)}$–$Mn_{3(b)}$, $Mn_{4(a)}$–$O_{(5)}$ and $Mn_{3(b)}$–$O_{(5)}$ distances were 2.98(2.91), 2.33(2.34), 2.03(2.02) and 0.20(0.19) (Å) respectively, where the corresponding values for B-monomer were given in parentheses. The $Mn_{4(a)}$–$Mn_{3(b)}$ distances estimated by using the observed $Mn_{4(a)}$–$O_{(5)}$ distance for 5GTHA(B) were 2.88(2.88) and 2.84(2.84) (Å) for $O_{(5)}$=OH^- and O^{2-}, respectively. On the other hand, the $Mn_{4(a)}$–$O_{(5)}$ distances estimated by using the observed $Mn_{4(a)}$–$Mn_{3(b)}$ distance for

Table 4. The calculated Mn_4-Mn_3 distances [Å] of the XFEL[27] and SFX[28,29] structures of the $CaMn_4O_5$ cluster of OEC of PSII based on the $Mn_{4(a)}$–$O_{(5)}$ distances [Å] shortened by the corrections of the XFEL expansions.[a]

Structures	Distance[b]		Duration	Time			
		0 fs	10 fs	a fs	b fs	50 fs	
Difference (Δ)		0%	2.13%	5%	10%	24.4%	Type
4UB6A	$Mn_{4(a)}$–$O_{(5)}$	2.32	2.27	2.20	2.09	1.75	
	$Mn_{4(a)}$–$Mn_{3(b)}$	2.87	2.85	2.81	2.75		$O_{(5)}$=OH^-
	$Mn_{4(a)}$–$Mn_{3(b)}$	2.84	2.82	2.81	2.78	2.69	$O_{(5)}$=O^{2-}
4UB6B	$Mn_{4(a)}$–$O_{(5)}$	2.30	2.25	2.19	2.07	1.74	
	$Mn_{4(a)}$–$Mn_{3(b)}$	2.86	2.84	2.81	2.76		$O_{(5)}$=OH^-
	$Mn_{4(a)}$–$Mn_{3(b)}$	2.83	2.82	2.81	2.78	2.69	$O_{(5)}$=O^{2-}
4UB8A	$Mn_{4(a)}$–$O_{(5)}$	2.38	2.33	2.26	2.14	1.80	
	$Mn_{4(a)}$–$Mn_{3(b)}$	2.90	2.88	2.84	2.78		$O_{(5)}$=OH^-
	$Mn_{4(a)}$–$Mn_{3(b)}$	2.85	2.84	2.82	2.79	2.70	$O_{(5)}$=O^{2-}
4UB8B	$Mn_{4(a)}$–$O_{(5)}$	2.33	2.28	2.21	2.10	1.76	
(5GTHA)[c]	$Mn_{4(a)}$–$Mn_{3(b)}$	2.88	2.85	2.82	2.76		$O_{(5)}$=OH^-
(5KAFA(B))[c]	$Mn_{4(a)}$–$Mn_{3(b)}$	2.84	2.83	2.81	2.78	2.69	$O_{(5)}$=O^{2-}
(5GTHB)[c]	$Mn_{4(a)}$–$O_{(5)}$	2.34	2.29	2.22	2.11	1.82	
	$Mn_{4(a)}$–$Mn_{3(b)}$	2.88	2.85	2.82	2.76		$O_{(5)}$=OH^-
	$Mn_{4(a)}$–$Mn_{3(b)}$	2.84	2.83	2.81	2.78	2.69	$O_{(5)}$=O^{2-}
5WS5A(B)	$Mn_{4(a)}$–$O_{(5)}$	2.29	2.24	2.18	2.06	1.73	
	$Mn_{4(a)}$–$Mn_{3(b)}$	2.86	2.84	2.81	2.76		$O_{(5)}$=OH^-
	$Mn_{4(a)}$–$Mn_{3(b)}$	2.83	2.82	2.81	2.78	2.69	$O_{(5)}$=O^{2-}

[a] The $Mn_{4(a)}$–$O_{(5)}$ distances of the XFEL structures[27] were estimated by using the Coulomb explosion distance (Δ_{XFEL}) in Equation (11). [b] The $Mn_{4(a}$–$Mn_{3(b)}$ distances were estimated by using Equations (2) and (3) under the assumption of a1) $O_{(5)}$=OH^- and a2) $O_{(5)}$=O^{2-}. [c] The $Mn_{4(a)}$–$O_{(5)}$ distances for 5GTHA(B)[28] and 5KAFA(B)[29] by SFX were the same as that of 4UB8B, providing the same estimation results.

Table 5. The Mn_4–Mn_3 distances [Å] of the $CaMn_4O_5$ cluster in the S_1 state of OEC of PSII by SFX[28,29] with and without preflash and estimation procedure [Eqs. (2) and (3)].

Structures	Mn_4–Mn_3 XRD	Mn_4–Mn_3[a] (Estimation)	Mn_4–$O_{(5)}$[b] Exp.(Est.)	Mn_3–$O_{(5)}$[c] Exp.	$O_{(5)}$[d]	SSB[e]	Topology[f]
5GTHA	2.98	(2.88)[a1]	2.33	2.03	$O_{(5)}$=OH^-	0.20	C_R
(no preflash		(2.84)[a2]	2.33	2.03	$O_{(5)}$=O^{2-}	0.20	C_R
dark SFX)	2.98		(2.54)[b1]	(2.0)[c1]	$O_{(5)}$=OH^-	−0.01	C
	2.98		(2.90)[b2]	(1.8)[c2]	$O_{(5)}$=O^{2-}	−0.37	C_L
5GTHB	2.91	(2.88)[a1]	2.34	2.02	$O_{(5)}$=OH^-	0.19	C_R
(no preflash		(2.84)[a2]	2.34	2.02	$O_{(5)}$=O^{2-}	0.19	C_R
dark SFX)	2.91		(2.40)[b1]	(2.0)[c1]	$O_{(5)}$=OH^-	0.13	C_R
	2.91		(2.62)[b2]	(1.8)[c2]	$O_{(5)}$=O^{2-}	−0.09	C
5WS5A	2.77	(2.86)[a1]	2.29	2.02	$O_{(5)}$=OH^-	0.24	C_R
(preflash dark		(2.83)[a2]	2.29	2.02	$O_{(5)}$=O^{2-}	0.24	C_R
SFX)	2.77		(2.12)[b1]	(2.0)[c1]	$O_{(5)}$=OH^-	0.41	R
	2.77		(2.06)[b2]	(1.8)[c2]	$O_{(5)}$=O^{2-}	0.47	R
5WS5B	2.75	(2.86)[a1]	2.29	2.03	$O_{(5)}$=OH^-	0.24	C_R
(preflash dark		(2.83)[a2]	2.29	2.03	$O_{(5)}$=O^{2-}	0.24	C_R
SFX)	2.75		(2.08)[b1]	(2.0)[c1]	$O_{(5)}$=OH^-	0.45	R
	2.75		(1.98)[b2]	(1.8)[c2]	$O_{(5)}$=O^{2-}	0.55	R
5KAFA(B)	2.87	(2.88)	2.33	2.20	$O_{(5)}$=OH^-	0.20	C_R
(no preflash		(2.84)	2.33	2.20	$O_{(5)}$=O^{2-}	0.20	C_R
dark SFX)	2.87		(2.32)	(2.0)	$O_{(5)}$=OH^-	0.21	C_R
	2.87		(2.46)	(1.8)	$O_{(5)}$=O^{2-}	0.07	C

[a] The $Mn_{4(a)}$–$Mn_{3(b)}$ distances were estimated by using the experimental $Mn_{4(a)}$–$O_{(5)}$ distance by SFX structures[28,29] with and without preflash in Equations (2) and (3) under the assumption of a1) $O_{(5)}$=OH^- and a2) O^{2-}. [b] The $Mn_{4(a)}$–$O_{(5)}$ distances were estimated by using the experimental $Mn_{4(a)}$–$Mn_{3(b)}$ distance in Equations (2) and (3) under the assumption of b1) $O_{(5)}$=OH^- and b2) O^{2-}. [c] The $Mn_{3(b)}$–$O_{(5)}$ distances were estimated to be 2.0 and 1.8 for c1) $O_{(5)}$=OH^- and c2) O^{2-}, respectively. [d] Assignment of the $O_{(5)}$ site. [e] Structural symmetry breaking (SSB) parameter. [f] Topology.

5GTHA(B) were 2.54(2.40) and 2.90(2.62) (Å) for $O_{(5)}$=OH^- and O^{2-}, respectively. The estimated $Mn_{4(a)}$–$O_{(5)}$ distances supported $O_{(5)}$=OH^-. The structural parameters for 5GTHA(B) without preflash were fully consistent with those of previous SFX structure without preflash.[27] They were also compatible with 5KAFA(B) structure without preflash by Young et al.,[29] the structure of A monomer by LD XRD[30] and the reassigned EXAFS structure (see Tables S6 and S7).[39]

The SFX results for A(B)-monomer of 5WS5 with preflash[28] indicated that the $Mn_{4(a)}$-$Mn_{3(b)}$, $Mn_{4(a)}$–$O_{(5)}$ and $Mn_{3(b)}$–$O_{(5)}$ distances for were 2.77(2.75), 2.29(2.29), 2.02(2.03) and 0.24(0.24) (Å), respectively. The $Mn_{4(a)}$–$Mn_{3(b)}$ distances estimated by using the observed $Mn_{4(a)}$–$O_{(5)}$ distance for 5WS5A(B) were 2.86(2.86) and 2.83(2.83) (Å) for $O_{(5)}$=OH^- and O^{2-}, respectively. The estimated $Mn_{4(a)}$–$Mn_{3(b)}$ distances were longer by about 0.1 Å than the corresponding observed values. On the other hand, the $Mn_{4(a)}$–$O_{(5)}$ distances estimated by using the observed $Mn_{4(a)}$–$Mn_{3(b)}$ distance for 5WS5A(B) with preflash were 2.12(2.08) and 2.06(1.98) (Å) for $O_{(5)}$=OH^- and O^{2-}, respectively. The estimated $Mn_{4(a)}$–$O_{(5)}$H distances were shorter by about 0.2 Å than the observed value, indicating the similarity to the corresponding observed values of B-monomer of LD XRD.[30] Moreover, the $Mn_{4(a)}$–$O_{(5)}$ distance estimated by 5% reduction of the observed values of 5WS5A(B) by SFX(SACLA) is 2.18(2.18) which is in compatible with those of the B-monomer of LD XRD at 1.85 Å resolution as shown in Table 4. Judging from the estimated $Mn_{4(a)}$–$O_{(5)}$ distances, and the observed $Mn_{4(a)}$–$Mn_{3(b)}$ and $Mn_{3(b)}$–$O_{(5)}$ distances, 5WS5A(B) structure with preflash was similar to B-monomer of LD XRD.[30] Preflash effect was significant for successive investigation of the S_1-to-S_3 transition investigated by SFX.[28,29] Further examinations of the SFX results after two flash illuminations were given in the Section SV in the Supporting Information (Table S8).

4.4. Importance of Hydrogen-Bonding Interactions in the Protein Field

Subtle structural differences between A- and B-monomers by low-dose XRD[30] were examined for elucidation of important roles of the environmental effects around the $CaMn_4O_5$ cluster. Figure 4 illustrates the observed Mn-O distances, together with hydrogen bonding interactions for the $CaMn_4O_5$ cluster. The $O_{(3)}$–N(His 337) distances for 5B5EA(5B66A) and 5B5EB(5B66B) were 2.46(2.48) and 2.75(2.74) (Å), respectively. The $O_{(3)}$-N distances of the A-monomers are shorter by 0.29(0.26) Å than those of the B-monomers, indicating that the $O_{(3)}$–H–N(His 337) hydrogen bonding interaction[30] is very strong for the A-monomers. The $Mn_{3(b)}$–$O_{(3)}$ bond lengths for 5B5EA(5B66A) and 5B5EB(5B66B) were 2.27(2.18) and 1.96(1.95) (Å), respectively. The $Mn_{3(b)}$–$O_{(3)}$ distances of the A-monomers are longer by 0.31(0.23) Å than those of the B-monomers, indicating the elongation induced by the strong hydrogen bonding interaction.[30]

The $O_{(4)}$–$O_{(11)}$(W11) distances for 5B5EA(5B66A) and 5B5EB(5B66B) were 2.66(2.71) and 2.44(2.45) (Å), respectively. The $O_{(4)}$–$O_{(11)}$ distances of the B-monomers are shorter by 0.22(0.26) Å than those of the A-monomers, indicating very strong $O_{(4)}$–H–$O_{(11)}$(W11) hydrogen bonding interaction. The $Mn_{4(a)}$–$O_{(4)}$ bond lengths for 5B5EA(5B66A) and 5B5EB(5B66B) were 1.87(1.84) and 2.07(2.10) (Å), respectively. The $Mn_{4(a)}$–$O_{(4)}$ distances of the B-monomers are longer by 0.20(0.26) Å than those of the A-monomers, indicating the elongation induced by the very strong hydrogen bonding interaction. The elongation of the $Mn_{4(a)}$–$O_{(4)}$ distance is consistent with the JT distortion in Figure 1 B.[38] Thus, the LD XRD experiments[30] opened the door for understanding important roles of confinement effects[37,45] of protein such as hydrogen bonding networks for subtle geometry changes of the $CaMn_4O_5$ cluster in OEC of PSII, indicating the following structural fluctuations ($\Delta R_{protein} <$ 0.1 Å) depending on states of protein fields [Eq. (12)]:

$$R(Mn_{4(a)}-Mn_{3(b)})_{protein} = 2.80 \pm \Delta R_{protein}(Å) \quad (12)$$

The large-scale QM/MM models involving hydrogen bonding networks[36–38] are necessary for theoretical investigation of $\Delta R_{protein}$ at the atomic level for the $CaMn_4O_5$ cluster controlled by several environmental effects,[1,2] such as pH,[54] hydrogen bonding and packing structures[27–30] of OEC of PSII.

4.5. Implication of Present Results in Artificial Photosynthesis

The $CaMn_4O_5$ cluster in OEC of PSII examined here is a roadmap for artificial photosynthesis. Present results indicate importance of design of appropriate reaction fields for the purpose.[36–39] Hole-doped Mn oxides such as the $CaMn_4O_5$ cluster[33–35] are typical strongly correlated electron systems (SCES),[39] for which orbital, charge and spin degrees of freedom play important roles for emergence of various important properties and functions such as magneto-resistance,[55] single molecule magnets[56] and spin frustration.[57] We have already investigated the charge and spin degrees of the $CaMn_4O_5$ cluster[33–39] in relation to the mixed-valence (MV) states revealed by EXAFS[2–11] and ground spin states observed by EPR.[1,44] In this paper, the orbital degree of freedom and related Jahn–Teller (JT) deformation of the $CaMn_4O_5$ cluster were investigated to elucidate possible origins of the two different geometrical structures by low dose (LD) XRD.[30] Hydrogen bonding networks around the $CaMn_4O_5$ cluster play important roles for subtle regulation of its geometrical structures.

Present theoretical results in turn indicate that SCES such as magnetic transition-metal clusters developed in the field of molecular magnetism[55–57] may be converted into active catalysts for water oxidation in artificial photosynthesis, as proposed previously.[35,58,59] To this end, the $CaMn_4O_5$ cluster in OEC of PSII can be replaced with other SCESs constructed of abundant 3d transition metals such as Fe, Co, Cu etc. for development of artificial photo-catalysts for which precious metals have been used for catalytic sites. Protein field is also replaced with other robust confinement materials such as metal organic framework (MOF), polyoxo metallate (POM), nanotube (NT) as illustrated in Figure 5.[35,58,59] Masaoka et al.[60] very recently made a great breakthrough for conversion of the Fe_5 magnetic cluster[57] into an active catalyst for water conversion by electrochemical hole-doping techniques. Design of appropriate ligands[35,58,59] for hole doping by solar energy are desirable for future developments of molecular catalysts for water oxidation.

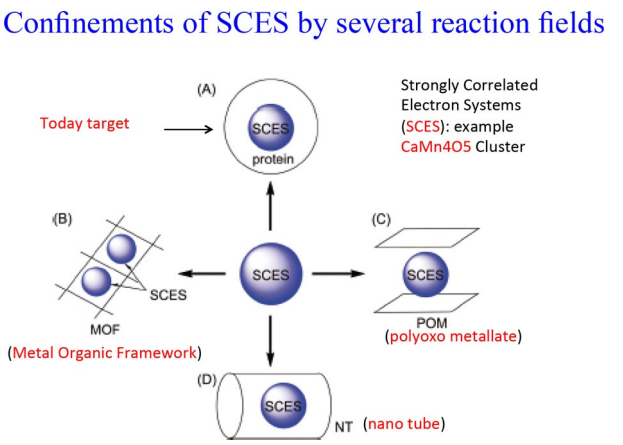

Figure 5. Our theoretical proposal of artificial photosynthesis where the protein field of OEC of PSII confines the $CaMn_4O_5$ cluster which is a typical example of hole-doped strongly correlated electron systems (SCES).[33] The $CaMn_4O_5$ cluster can be replaced with other SCESs constructed of abundant 3d transition, such as, for example, Mn, Fe, and Co. The protein field is replaced with other confinement materials, such as metal–organic frameworks (MOF), polyoxometallates (POM) and nanotubes (NT).

5. Conclusions

The JT deformation formula[37–39] are found to be useful and applicable for understanding and qualitative prediction of JT deformations of the $CaMn_4O_5$ cluster in OEC of PSII. In fact, the JT deformation formula[37–39] was successfully applied for elucidation of structural deformations of the $CaMn_4O_5$ cluster in the A- and B-monomers of the dimer structure of PSII by the XRD experiments under low dose 0.03 MGy (5B5E) and 0.12 MGy (5B66) conditions.[30] The $Mn_{3(b)}$–$Mn_{4(a)}$, $Mn_{4(a)}$–$O_{(5)}$ and $Mn_{3(b)v}O_{(5)}$ distances of the A-monomer are about 2.8, 2.2 and 2.0 (Å) respectively, showing the JT (d_{x^2}) elongation of the $Mn_{4(a)}$–$O_{(5)}$ distance responsible for the C_R structure in Figure 1 C. The corresponding distances of the B-monomer are 2.75, 2.1 and 2.0 (Å) respectively, indicating the JT (d_{y^2}) deformation (see Figure 1 B). The structure of the A-monomer by LD XRD[30] is consistent with the refined SFX structure without XFEL damage[27–29] (see Table 4) and the reassigned EXAFS[37–39] structures, whereas the structure of the B-monomer by LD XRD is compatible with the original EXAFS structure[10] (see Table S5) and the recent SFX structure with preflash[28] (see Table 5). The EXAFS structure[10] has been referred to as the reference structure to support the theoretical S_1 models with the vertical JT (d_{z^2}) deformation (see Figure 1 A), for which the $Mn_{3(b)}$–$Mn_{4(a)}$, $Mn_{4(a)}$–$O_{(5)}$ and $Mn_{3(b)}$–$O_{(5)}$ distances are 2.7, 1.8 and 1.8 (Å), respectively. The last structure[40] is therefore similar to the R-opened S_2 structure of the $CaMn_4O_5$ cluster.[35–37] Thus the LD XRD structures[30] have provided structural foundations for reasonable explanation and understanding of the XRD,[3–10] XFEL,[27–29] EXAFS[8,10] structures and computational models[33–47] in the S_1 state of OEC of PSII. In conclusion, the $CaMn_4O_5$ cluster in OEC of PSII is labile[33] for catalytic water oxidation, exhibiting subtle geometry changes induced by hydrogen bonding interactions, JT effects of the Mn^{III} ion and other environmental effects such as pH[55] and packing structures.[27–30] Large-scale QM/MM calculations[37,38] were necessary for elucidation of subtle structural fluctuations of the $CaMn_4O_5$ cluster by the protein field of PSII at atomic scale. The JT deformation formulae were successfully applied for theoretical analysis of the recent SFX results[28,29] after two flash (see Section SV in the Supporting Information). Finally, implications of the present results for artificial photosynthesis by the use of abundant transition metals[56–60] have been touched briefly.

Acknowledgements

This work has been supported by a Grants-in-Aid for Scientific Research on Innovative Areas No. 17H06433 (to NK and KY) and by the Ministry of Education, Culture, Sports, Science and Technology (MEXT) of Japan.

Conflict of Interest

The authors declare no conflict of interest.

Keywords: artificial photosynthesis · oxygen evolving complex · photosystem II · theoretical models · X-ray diffraction

[1] D. J. Vinyard, G. M. Ananyew, G. C. Dismukes, *Annu. Rev. Biochem.* **2013**, *82*, 577 – 606.
[2] J. Yano, V. K. Yachandra, *Chem. Rev.* **2014**, *114*, 4175 – 4205.
[3] V. K. Yachandra, K. Sauer, M. P. Klein, *Chem. Rev.* **1996**, *96*, 2927 – 2950.
[4] R. M. Cinco, K. L. M. Holman, J. H. Robblee, J. Yano, S. A. Pizarro, E. Bellacchio, K. Sauer, V. K. Yachandra, *Biochemistry* **2002**, *41*, 12928 – 12933.
[5] H. Dau, P. Liebisch, M. Haumann, *Phys. Chem. Chem. Phys.* **2004**, *6*, 4781 – 4792.
[6] J. Yano, J. Kern, K.-D. Irrgang, M. J. Latimer, U. Bergmann, P. Glatzel, Y. Pushkar, J. Biesiadka, B. Loll, K. Sauer, J. Messinger, A. Zouni, V K. Yachandra, *Proc. Natl. Acad. Sci. USA* **2005**, *102*, 12047 – 12052.
[7] M. Grabolle, H. Haumann, C. Muller, P. Liebisch, H. Dau, *J. Biol. Chem.* **2006**, *281*, 4580 – 4588.
[8] J. Yano, J. Kern, K. Sauer, M. J. Latimer, Y. Pushkar, J. Biesiadka, B. Loll, W. Saenger, J. Messinger, A. Zouni, V. K. Yachandra, *Science* **2006**, *314*, 821 – 825.
[9] A. Grundmeier, H. Dau, *Biochim. Biophys. Acta Bioenerg.* **2012**, *1817*, 88 – 105.
[10] G. Glöckner, J. Kern, M. Broser, A. Zouni, V. Yachandra, J. Yano, *J. Biol. Chem.* **2013**, *288*, 22607 – 22620.
[11] K. Ferreira, T. Iverson, K. Maghlaoui, J. Baber, S. Iwata, *Science* **2004**, *303*, 1831 – 1838.
[12] J. Biesiadka, B. Loll, J. Kern, K. D. Irrgang, A. Zouni, *Phys. Chem. Chem. Phys.* **2004**, *6*, 4733 – 4736.
[13] B. Loll, J. Kern, W. Saenger, A. Zouni, J. Biesiadka, *Nature* **2005**, *438*, 1040 – 1044.
[14] R. Krivanek, J. Kern, A. Zouni, H. Dau, M. Haumann, *Biochim. Biophys. Acta Bioenerg.* **2007**, *1767*, 520 – 527.
[15] A. Guskov, J. Kern, A. Gabdulkhakov, M. Broser, A. Zouni, W. Saenger, *Nat. Struct. Mol. Biol.* **2009**, *16*, 334 – 342.
[16] K. Kawakami, Y. Umena, N. Kamiya, J. R. Shen, *Proc. Natl. Acad. Sci. USA* **2009**, *106*, 8567 – 8572.
[17] A. Guskov, A. Gabdulkhakov, M. Broser, C. Glockner, J. Hellmich, J. Kern, J. Frank, F. Muh, W. Saenger, A. Zouni, *ChemPhysChem* **2010**, *11*, 1160 – 1171.
[18] Y. Umena, K. Kawakami, J. R. Shen, N. Kamiya, *Nature* **2011**, *473*, 55 – 60.
[19] K. Kawakami, Y. Umena, N. Kamiya, J. R. Shen, *J. Photochem. Photobiol. B* **2011**, *104*, 9 – 18.
[20] R. Neutze, R. Wouts, D. van der Spoel, E. Weckert, J. Hajdu, *Nature* **2000**, *406*, 752 – 757.

[21] H. N. Chapman, P. Fromme, A. Barty, T. A. White, R. A. Kirian, A. Aquila, M. S. Hunter, J. Schulz, D. P. DePonte, U. Weierstall, R. B. Doak, F. R. N. C. Maia, A. V. Martin, I. Schlichting, L. Lomb, N. Coppola, R. L. Shoeman, S. W. Epp, R. Hartmann, D. Rolles, A. Rudenko, L. Foucar, N. Kimmel, G. Weidenspointner, P. Holl, M. Liang, M. Barthelmess, C. Caleman, S. Boutet, M. J. Bogan, J. Krzywinski, C. Bostedt, S. Bajt, L. Gumprecht, B. Rudek, B. Erk, C. Schmidt, A. Homke, C. Reich, D. Pietschner, L. Struder, G. Hauser, H. Gorke, J. Ullrich, S. Hermann, G. Schaller, F. Schopper, H. Soltau, K.-U. Kuhnel, M. Messerschmidt, J. D. Bozek, S. P. Hau-Riege, M. Frank, C. V. Hampton, R. G. Sierra, D. Starodub, G. J. Williams, J. Hajdu, N. Timneanu, M. M. Seibert, J. Andreasson, A. Rocker, O. Jonsson, M. Svenda, S. Stern, K. Nass, R. Andritschke, C.-D. Schoter, F. Krasniqi, M. Bott, K. E. Schmidt, X. Wang, I. Grotjohann, J. M. Holton, T. R. M. Barends, R. Neutze, S. Marchesini, R. Fromme, S. Schorb, D. Rupp, M. Adolph, T. Gorkhover, I. Andersson, H. Hirsemann, G. Potdevin, H. Graafsma, B. Nilsson and J. C. H. Spence, *Nature* **2011**, *470*, 73 – 77.

[22] S. Boutet, L. Lomb, G. J. Williams, T. R. M. Barends, A. Aquila, R. B. Doak, U. Weierstall, D. P. DePonte, J. Steinbrener, R. L. Shoeman, M. Messerschmidt, A. Barty, T. A. White, S. Kassemeyer, R. A. Kirian, M. M. Seibert, R. A. Montanez, C. Kenney, R. Herbst, P. Hart, J. Pines, G. Haller, S. M. Gruner, T. H. Philipp, M. W. Tate, M. Hromalik, L. J. Koerner, N. van Bakel, J. Morse, W. Ghonsalves, D. Arnlund, M. J. Bogan, C. Caleman, R. Fromme, C. Y. Hampton, M. S. Hunter, L. C. Johansson, G. Katona, C. Kupitz, M. Liang, A. V. Martin, K. Nass, L. Redecke, F. Stellato, N. Tinneanu, D. Wang, N. A. Zatsepin, D. Schafer, J. Defever, R. Neutze, P. Fromme, J. C. H. Spence, H. N. Chapman, I. Schlichting, *Science* **2012**, *337*, 362 – 364.

[23] J. Kern, R. Alonso-Mori, R. Tran, J. Hattne, R. J. Gildea, N. Echols, C. Glockner, J. Hellmich, H. Laksmono, R. G. Sierra, B. Lassalle-Kaiser, S. Koroidov, A. Lampe, G. Han, S. Gul, D. DiFiore, D. Milathianaki, A. R. Fry, A. Miahnahri, D. W. Schafer, M. Messerschmidt, M. M. Seibert, J. E. Koglin, D. Sokaras, T.-C. Weng, J. Sellberg, M. J. Latimer, R. W. Grosse-Kunstleve, P. H. Zwart, W. E. White, P. Glatzel, P. D. Adams, M. J. Bogan, G. J. Williams, S. Boutet, J. Messinger, A. Zouni, N. K. Sauter, V. K. Yachandra, U. Bergmann, J. Yano, *Science* **2013**, *340*, 491 – 495.

[24] C. Kupitz, S. Basu, I. Grotjohann, R. Fromme, N. A. Zatsepin, K. N. Rendek, M. S. Hunter, R. L. Shoeman, T. A. White, D. Wang, D. James, J.-H. Yang, D. E. Cobb, B. Reeder, R. G. Sierra, H. Liu, A. Barty, A. L. Aquila, D. Deponte, R. A. Kirian, S. Bari, J. J. Bergkamp, K. R. Beyerlein, M. J. Bogan, C. Caleman, T.-C. Chao, C. E. Conrad, K. M. Davis, H. Fleckenstein, L. Galli, S. P. Hau-Riege, S. Kassemeyer, H. Laksmono, M. Liang, L. Lomb, S. Marchesini, A. V. Martin, M. Messerschmidt, D. Milathianaki, K. Nass, A. Ros, S. Roy-Chowdhury, K. Schmidt, M. Seibert, J. Steinbrener, F. Stellato, L. Yan, C. Yoon, T. A. Moore, A. L. Moore, Y. Pushkar, C. J. Williams, S. Boutet, R. B. Doak, U. Weierstall, M. Frank, H. N. Chapman, J. C. H. Spencer, P. Fromme, *Nature* **2014**, *513*, 261 – 265.

[25] J. Kern, R. Tran, R. Alonso-Mori, S. Koroidov, N. Echols, J. Hattne, M. Ibrahim, S. Gul, H. Laksmono, R. G. Sierra, R. J. Gildea, G. Han, J. Hellmich, B. Lasalle-Kaiser, R. Chatterjee, A. S. Brewster, C. A. Stan, C. Glockner, A. Lampe, D. DiFiore, D. Milathianaki, A. R. Fry, M. M. Seibert, J. E. Koglin, E. Gallo, J. Uhlig, D. Sokaras, T.-C. Weng, P. H. Zwart, D. E. Skinner, M. J. Bogan, M. Messerschmidt, P. Glatzel, G. J. Williams, S. Boutet, P. D. Adams, A. Zouni, J. Messinger, N. K. Sauter, U. Bergmann, J. Yano, V. K. Yachandra, *Nat. Commun.* **2014**, *5*, 4371.

[26] K. Hirata, K. Shinzawa-Itoh, N. Yano, S. Takemura, K. Kato, M. Hatanaka, K. Muramoto, T. Kawahara, T. Tsukihara, E. Yamashita, K. Tono, G. Ueno, T. Hikima, H. Murakami, Y. Inubushi, M. Yabashi, T. Ishikawa, M. Yamamoto, T. Ogura, H. Sugimoto, J.-R. Shen, S. Yoshikawa, H. Ago, *Nat. Methods* **2014**, *11*, 734 – 736.

[27] M. Suga, F. Akita, K. Hirata, G. Ueno, H. Murakami, Y. Nakajima, T. Shimizu, K. Yamashita, M. Yamamoto, H. Ago, J.-R. Shen, *Nature* **2015**, *517*, 99 – 103.

[28] M. Suga, F. Akita, M. Sugahara, M. Kubo, Y. Nakajima, T. Nakane, K. Yamashita, Y. Umena, M. Nakabayashi, T. Yamane, T. Nakano, M. Suzuki, T. Masuda, S. Inoue, T. Kimura, T. Nomura, S. Yonekura, L.-J. Yu, T. Sakamoto, T. Motomura, J.-H. Chen, Y. Kato, T. Noguchi, K. Tono, Y. Joti, T. Kameshima, T. Hatsui, E. Nango, R. Tanaka, H. Naitow, Y. Matsuura, A. Yamashita, M. Yamamoto, O. Nureki, M. Yabashi, T. Ishikawa, S. Iwata, J.-R. Shen, *Nature* **2017**, *543*, 131 – 135.

[29] I. D. Young, M. Ibrahim, R. Chatterjee, S. Gul, F. D. Fuller, S. Koroidov, A. S. Brewster, R. Tran, R. Alonso-Mori, T. Kroll, T. Michels-Clark, H. Laksmono, R. G. Sierra, C. A. Stan, R. Hussein, M. Zhang, L. Douthit, M. Kubin, C. de Lichtenberg, L. V. Pham, H. Nilsson, M. H. Cheah, D. Shevela, C. Saracini, M. A. Bean, I. Seuffert, D. Sokaras, T.-C. Weng, E. Pastor, C. Weninger, T. Fransson, L. Lassalle, P. Brauer, P. Aller, P. T. Docker, B. Andi, A. M. Orville, J. M. Glownia, S. Nelson, M. Sikorski, D. Zhu, M. S. Hunter, T. J. Lane, A. Aquila, J. E. Koglin, J. Robinson, M. Liang, S. Bouter, A. Y. Lyubimov, M. Uervirojnangkoorn, N. W. Moriarty, D. Liebschner, P. V. Afonine, D. G. Waterman, G. Evans, P. Wernet, H. Dobbek, W. I. Weis, A. T. Brunger, P. H. Zwart, P. D. Adams, A. Zouni, J. Messinger, U. Bergmann, N. K. Sauter, J. Kern, V. K. Yachandra, J. Yano, *Nature* **2016**, *540*, 453 – 457.

[30] A. Tanaka, Y. Fukushima, N. Kamiya, *J. Am. Chem. Soc.* **2017**, *139*, 1718 – 1721.

[31] P. Joliot, *Biochim. Biophys. Acta* **1965**, *102*, 116 – 134.

[32] B. Kok, B. Forbush, M. McGloin, *Photochem. Photobiol.* **1970**, *11*, 457 – 475.

[33] K. Kanda, S. Yamanaka, T. Saito, Y. Umena, K. Kawakami, J. R. Shen, N. Kamiya, M. Okumura, H. Nakamura, K. Yamaguchi, *Chem. Phys. Lett.* **2011**, *506*, 98 – 103.

[34] S. Yamanaka, H. Isobe, K. Kanda, T. Saito, Y. Umena, K. Kawakami, J. R. Shen, N. Kamiya, M. Okumura, H. Nakamura, K. Yamaguchi, *Chem. Phys. Lett.* **2011**, *511*, 138 – 145.

[35] H. Isobe, M. Shoji, S. Yamanaka, Y. Umena, K. Kawakami, N. Kamiya, J.-R. Shen, K. Yamaguchi, *Dalton Trans.* **2012**, *41*, 13727 – 13740.

[36] M. Shoji, H. Isobe, S. Yamanaka, Y. Umena, K. Kawakami, N. Kamiya, J.-R. Shen, K. Yamaguchi, *Catal. Sci. Technol.* **2013**, *3*, 1831 – 1848.

[37] M. Shoji, H. Isobe, S. Yamanaka, Y. Umena, K. Kawakami, N. Kamiya, J.-R. Shen, T. Nakajima, K. Yamaguchi, *Adv. Quant. Chem.* **2015**, *70*, 325 – 413.

[38] M. Shoji, H. Isobe, T. Nakajima, K. Yamaguchi, *Chem. Phys. Lett.* **2016**, *658*, 354 – 363.

[39] K. Yamaguchi, M. Shoji, H. Isobe, S. Yamanaka, Y. Umena, K. Kawakami, N. Kamiya, *Mol. Phys.* **2017**, *115*, 636 – 666.

[40] P. E. M. Siegbahn, *J. Photochem. Photobiol. B* **2011**, *104*, 94 – 99.

[41] I. Rivalta, G. R. Brudvig, V. S. Batsita, *Curr. Opin. Chem. Biol.* **2012**, *16*, 11 – 18.

[42] A. Galstyan, A. Robertazzi, E. W. Knapp, *J. Am. Chem. Soc.* **2012**, *134*, 7442 – 7449.

[43] P. Gatt, S. Petrie, R. Stranger, R. J. Pace, *Angew. Chem. Int. Ed.* **2012**, *51*, 12025 – 12028; *Angew. Chem.* **2012**, *124*, 12191 – 12194.

[44] V. Krewald, M. Retagan, N. Cox, J. Messinger, W. Lubitz, S. Debeer, F. Neese, D. A. Pantazis, *Chem. Sci.* **2015**, *6*, 1676 – 1695.

[45] K. Yamaguchi, S. Yamanaka, M. Shoji, H. Isobe, Y. Kitagawa, T. Kawakami, S. Yamada, M. Okumura, *Mol. Phys.* **2014**, *112*, 485 – 507.

[46] J. Wang, M. Askera, G. W. Brudvig, V. S. Batista, *ACS Energy Lett.* **2017**, *2*, 397 – 407.

[47] S. Petrie, R. Stranger, R. J. Pace, *Phys. Chem. Chem. Phys.* **2017**, *19*, 27682 – 27693.

[48] M. Shoji, H. Isobe, S. Yamanaka, M. Suga, F. Akita, J.-R. Shen, K. Yamaguchi, *Chem. Phys. Lett.* **2015**, *627*, 44 – 52.

[49] K. Nagaya, K. Motoyama, E. Kukk, H. Fukuzawa, S. Wada, T. Tachibana, Y. Ito, S. Mondal, T. Sakai, K. Matsunami, R. Koga, S. Ohmura, Y. Takahashi, M. Kanno, A. Rudenko, C. Nicolas, X.-J. Liu, Y. Zhang, J. Chen, M. Anand, Y. H. Jiang, D. E. Kim, T. Tono, M. Yabashi, H. Kono, C. Miron, M. Yao, K. Ueda, *Phys. Rev. X* **2016**, *6*, 021035.

[50] K. Nagaya, K. Motomura, E. Kukk, Y. Takahashi, K. Yamazaki, S. Ohmura, H. Fukuzawa, S. Wada, S. Mondal, T. Tachibana, Y. Ito, R. Koga, T. Sakai, K. Matsunami, K. Nakamura, M. Kanno, A. Rudenko, C. Nicolas, X.-J. Liu, C. Miron, Y. Zhang, Y. Jiang, J. Chen, M. Anand, D. E. Kim, K. Tono, M. Yabashi, M. Yao, H. Kono, K. Ueda, *Faraday Discuss.* **2016**, *194*, 537 – 562.

[51] M. Amin, A. Badawi, S. S. Obayya, *Sci. Rep.* **2016**, *6*, 36492.

[52] M. Amin, M. Askerka, V. S. Batista, G. W. Brudvig, M. R. Gunner, *J. Phys. Chem. B* **2017**, *121*, 9382 – 9388.

[53] T. Ishikawa, H. Aoyagi, T. Asaka, Y. Asano, N. Azumi, T. Bizen, H. Ego, K. Fukami, T. Fukui, Y. Fukazawa, S. Goto, H. Hanaki, T. Hara, T. Hasegawa, T. Hatsui, A. Higashiya, T. Hirono, N. Hosoda, M. Ishii, T. Inagaki, Y. Inubushi, T. Itoga, Y. Joti, M. Kago, T. Kameshima, H. Kimura, Y. Kirihara, A. Kiyomichi, T. Kobayashi, C. Kondo, T. Kudo, H. Maesaka, X. M. Marechal, T. Masuda, S. Matsubara, T. Masumoto, T. Matsushita, S. Matsui, M. Nagasono. N. Nariyama, H. Ohashi, T. Ohata, T. Ohshima, S. Ono, Y. Otake, C. Saji, T. Sakurai, T. Sato, K. Sawada, T. Seike, K. Shirasawa, T. Sugimoto, S. Suzuki, S. Takahashi, H. Takabe, K. Takeshita, K. Tamasaku, H. Tanaka, R.

Tanaka, T. Tanaka, T. Togashi, K. Togawa, A. Tokuhisa, H. Tomizawa, K. Tono, S. Wu, M. Yabashi, M. Yamaga, A. Yamashita, K. Yanagida, C. Zhang, T. Shintake, H. Kitamura, N. Kumagai, *Nat. Photon.* **2012**, *6*, 540 – 544.

[54] A. Robertazzi, A. Galstan, E. W. Knapp, *Biochim. Biophys. Acta Bioenerg.* **2014**, *1837*, 1316 – 1321.

[55] K. Yosida, *Phys. Rev.* **1957**, *107*, 396.

[56] K. Yamaguchi, S. Yamanaka, M. Nishio, Y. Takano, Y. Kitagawa, H. Nagao, Y. Yoshioka, *Theor. Chem. Acc.* **1999**, *102*, 328 – 345.

[57] R. Ishikawa, M. Nakano, A. Fuyuhiro, T. Takeuchi, S. Kimura, T. Kashiwagi, M. Hagiwara, K. Kindo, S. Kaizaki, S. Kawata, *Chem. Eur. J.* **2010**, *16*, 11139 – 11144.

[58] K. Yamaguchi, Y. Kitagawa, H. Isobe, M. Shoji, S. Yamanaka, M. Okumura, *Polyhedron* **2013**, *57*, 138 – 149.

[59] K. Yamaguchi, M. Shoji, H. Isobe, Y. Kitagawa, S. Yamada, T. Kawakami, S. Yamanaka, M. Okumura, *Polyhedron* **2013**, *66*, 228 – 244.

[60] M. Okamura, M. Kondo, R. Kuga, Y. Kurashige, T. Yanai, S. Hayami, V. K. K. Praneeth, M. Yoshida, K. Yoneda, S. Kawata, S. Masaoka, *Nature* **2016**, *530*, 465 – 468.

Manuscript received: September 14, 2017
Revised manuscript received: November 2, 2017
Accepted manuscript online: November 10, 2017
Version of record online: December 27, 2017

